DELFT UNIVERSITY OF TECHNOLOGY

REPORT 13-06

Towards Advanced One-Dimensional Numerical Models for Multiphase Flow in Pipelines

J.S.B. van Zwieten

ISSN 1389-6520

Reports of the Delft Institute of Applied Mathematics

Delft 2013

Summary

In this report we give an overview of models and discretisation techniques for the simulation of multiphase flow in long pipelines. Due to the size of the pipelines we focus on one-dimensional models, which are derived from three-dimensional conservation laws for mass, momentum and energy. All discussed one-dimensional models are hyperbolic, the most accurate ones are also non-conservative. We discuss the Discontinuous Galerkin Finite Element Method, which is a discretisation technique suitable for hyperbolic models, together with additional methods to handle discontinuities and non-conservative models. We apply the DG-FEM discretisation to a commonly used two-phase flow model and verify the results using two test cases. Several test cases, however, fail when one of the phases vanishes. We propose several solutions to resolve this problem.

Joost van Zwieten, the author of this report, is a PhD student at Delft University. He carries out his project for Shell. The project aims at defining the next generation of numerical schemes and solver for the numerical-physical modelling of multiphase flow transport through wells and pipeline-riser systems. Shell has their in-house dynamic model COMPAS to solve for the transient flow of gas, oil, and water. The current numerical scheme in COMPAS applies an approximate Riemann discretization on a collocated grid, with implicit time discretization using a Newton-Raphson solver. The solver can become slow under certain conditions, such as low flow with the generation and transport of terrain slugs in the low spots of the pipeline. Therefore the COMPAS numerics are currently upgraded to a finite volume discretization on a staggered grid, with implicit time integration using a segregated solver with tri-diagonal matrices. The PhD project is meant to track the latest developments of numerical schemes for multiphase pipeline transport, as available in the open literature. The PhD project will also define a new scheme that, if successful, can be implemented in COMPAS in the near future.

At Delft University the project is monitored by Duncan van der Heul, Kees Vuik, and Ruud Henkes.

At Shell the project is monitored by Benjamin Sanderse, Patricio Rosen Esquivel, and Ruud Henkes.

Contents

Chapter 1

Introduction

The oil and gas industry requires accurate simulation tools for the design and safe operation of pipeline systems. Unstable flow may cause problems at the receiving facilities, such as flooding of the separator or a compressor trip, and it may cause pipeline integrity problems (vibrations, fatigue). For example, unstable flow can occur when the gas flow is too slow to drag liquid through upward inclined pipe sections. Liquid slugs followed by compressed gas bubbles arise and typically travel with high velocity through the pipe.

Since the pipelines can have a length of more than hundred kilometers, simulation of a three-dimensional multiphase model is infeasible. Cross sectionally averaged one-dimensional multiphase models are derived, which are significantly simpler from the computational point of view, however, they require extra closure models to compensate for the averaging. The one-dimensional models should be able to predict the onset of unstable flow, correct slug length distributions, slug frequency et cetera. For applications involving automated control, the simulation should be performed in real-time [16].

In this chapter we present an overview of models and numerical schemes developed in the past thirty years. These schemes can be divided into coarse grid (Section 1.1) and flow regime capturing schemes (Section 1.2). In Section 1.3 we propose some possible improvements to the existing schemes.

1.1 Early models

The first models and numerical schemes of 1D multiphase flow models were developed for simulations of loss of coolant accidents in pressurised water reactors in the nuclear industry [3, 5]. These simulations are characterised by fast transients. The oil and gas industry, on the other hand, was interested in the simulation of slow transients corresponding to mass transport over a long period of time, up to weeks. Several commercial or in-house codes were developed to meet these requirements: OLGA [4] and LedaFlow [32] are commercially, with OLGA being the market leader. PeTra [31] has been a research tool, and parts of it are now available in OLGA. COMPAS [23] is the Shell in-house dynamic simulator.

1.1.1 Partial Differential Equations

All three models mentioned above are based on the two-fluid model [24]. The OLGA model comprises three equations for the conservation of mass of the three fields gas, liquid and liquid droplets in gas. The first version of OLGA did not include the droplet field, which caused a significant error in the approximation of the pressure drop in vertical annular flow.

The model consists of two momentum equations for the gas phase (gas and droplet fields) and liquid phase, and a slip relation for the gas and droplet velocities to account for gravity and drag forces. Furthermore, there is a single energy conservation equation and a volume equation in the form of a pressure evolution equation. As is usually done in the derivation of one-dimensional two-phase flow models, the pressure is assumed to be constant over a cross section. Both the gas and liquid phase are assumed to be compressible.

The PeTra model and software package [31] is an extension of the OLGA model. The model aims to restore some three-dimensional details, which are lost due to averaging. The model keeps track of seven fields: the three phases gas, oil and water and all mixtures (droplets and dispersions) of oil and water in the three phases. For all fields except the liquid-liquid dispersions a mass balance equations is used. For the liquid-liquid dispersions an explicit relation is used. There are three equations for the conservation of momentum of gas and droplets, oil and water dispersion and water and oil dispersion. Like in OLGA, there is a volume equation in the form of a pressure evolution and a total energy equation.

COMPAS [23] uses a slightly different, simplified approach in comparison with OLGA and PeTra. Like PeTra three phases are considered: gas, oil and water. For each phase a mass balance equation is solved. There is a single total momentum balance and the model is closed with respect to the phase velocity components by introducing two slip relations. Furthermore, there is a total energy balance.

1.1.2 Flow regimes

Being limited by computational power, the above mentioned models use very coarse grid with elements magnitudes larger than the diameter of the pipe. Many important features, such as slugs, rolls waves et cetera, are too small to be represented by such a coarse grid. The mentioned codes make heavily use of empirical modelling to compensate for this. Flow regime maps, see for instance Taitel and Dukler [48], are used to determine momentary flow behaviour at every point in the pipe based on the mass flow rates, pressure, temperature and pipe inclination. For a given flow regime, the friction of the fluid-fluid and fluid-wall interfaces and slip relations for bubbles and droplets, if taken into account, are empirically modelled.

1.1.3 Discretisation

The mentioned software packages use a first order Finite Difference or Finite Volume discretisation with some form of upwinding for stabilisation. When using an explicit time integration, the maximum allowed time step size for stable integration scales with the ratio of the mesh width and the largest absolute eigenvalue of the semi-discrete system. For the two-fluid model the largest eigenvalue is roughly equal to the speed of sound of the liquid phase. The maximum allowed time step would be orders of magnitudes smaller than the desired simulation times, even using a rather coarse mesh and it thus not practically feasible. Therefore, the mentioned codes use implicit time integration and a time step size restriction based on the phase velocities.

1.1.4 Numerical improvements

The models and schemes described above are rather diffusive and to be fast enough for real-time simulations [14]. In his PhD thesis, Flåtten [16] derived several schemes which reduce the amount of numerical diffusion. To increase the numerical accuracy (through decreasing

the numerical diffusion) Flåtten extended the AUSM-type schemes [36] for the Euler equations, which are based on a splitting of the flux in a convective and a pressure part, to the two-fluid equations [14]. The amount of diffusion that the scheme generates is comparable to Roe-type methods, while being computationally more efficient. However, the scheme introduces spurious oscillations in the neighbourhood of discontinuities, caused by omitting pressure variation in the numerical mass flux. Later, Evje and Flåtten [15] addressed this issue by applying a splitting of the mass flux into a pressure and volume fraction component. The pressure component is chosen to be diffusive, in order to reduce the oscillations, and the volume fraction component is equal to the AUSM-type flux.

Beside the spatial discretization, also a proper temporal discretization is needed While OLGA and PeTra use a fully or strongly implicit time discretisation, which eliminates the CFL-condition completely, Flåtten chooses a semi or weakly implicit scheme [15] where, roughly speaking, pressure waves are discretised implicitly and momentum and volume fraction waves explicitly. The resulting CFL-condition lowers to a convective CFL-condition, often magnitudes lower than the sonic CFL-condition. The scheme requires the solution of one relatively simple linear equation, hence it remains computationally efficient. Unfortunately, the diffusion of pressure waves increases for increasing time step size.

Wangensteen [53] studied specifically the numerical aspects of the transition from and to single phase flow for the incompressible two-fluid equations with constant mixture velocity and the compressible two-fluid equations on Eulerian grids. An incorrect choice of numerical flux could lead to an unstable system when a pipe becomes completely filled with water. Wangensteen derived a set of conditions for the numerical mass flux, e.g. an element must not be overfilled, and proposed a numerical flux satisfying those conditions based on a splitting of the mass flux in a mixture and slip component. The method is named Mixture Slip Flux Splitting (MSFS). Numerical experiments revealed that the method was less accurate than a Roe scheme. Therefore, Wangensteen combined both the MSFS and Roe methods into a hybrid scheme which is stable in the region of single phase flow and accurate otherwise.

In a series of simulations the onset of unstable flow due to varying inflow conditions was compared with the Viscous Kelvin Helmholtz stability analysis of the analytical incompressible two-fluid model. The simulations showed that the onset is very sensitive to numerical parameters and type of flux limiter.

Wangensteen derived an MSFS scheme for the compressible two-fluid equations, similar to the weakly implicit scheme derived by Evje and Flåtten [15], but on a staggered grid where mass and momentum grid points are shifted with respect to each other. In certain situations the method does not converge.

1.2 Towards flow regime and slug capturing

As mentioned above, in the early two-fluid models the flow regimes are modelled explicitly. This means that based on certain physical criteria (involving dimensionless numbers like the Reynolds number and the Froude number), the flow regime is selected (like stratified flow, slug flow, annular flow, and bubbly flow). For the selected flow regime specific closure relations are applied. These closure relations are among others for the wall friction, for the friction at the interface between phases, and for the entrainment of droplets and bubbles. One might wonder whether the two-fluid model, being derived from the three-dimensional conservation laws, is capable of generating the correct flow behaviour by itself. For instance, when assuming a stratified geometry, e.g. gas on top of liquid, and including liquid entrainment in the gas phase, it seems possible to describe a slug quite reasonably. If the model is also capable of generating the slugs, then there would be no need for the explicit modelling

of friction and slip relations based on an estimation of a flow regime.

The Kelvin-Helmholtz instability is one of several mechanism which initiate slugs. Issa and Kempf [26] demonstrated the ability of the isentropic two-fluid model, with compressible gas phase and incompressible liquid phase, to capture the Kelvin-Helmholtz instability and generate slugs when using a discretisation accurate enough to describe waves with short wavelengths. Empirical modelling was only used for the friction of the fluid-fluid and fluid-wall interfaces. Furthermore, the model is capable of growing, merging and collapsing slugs, without extra empirical modelling.

Issa and Kempf observed that the onset and growth of instabilities are very sensitive to liquid-wall friction models, some of which even fail to produce slugs. By tuning the the friction model, the observed flow regimes of various simulations of a horizontal and slightly downward inclined pipe corresponded quite well with the flow pattern maps by Taitel and Dukler [48] for stratified and slug flow.

Bonizzi, Andreussi and Banerjee [7] went one step further by trying to capture more flow regimes, an attempt to come on par with OLGA, PeTra and COMPAS in terms of applicability, yet limited to near-horizontal pipelines. Compared to Issa and Kempf [26] the model is extended with the flow regimes annular and bubbly. Similar to the PeTra model, the two-fluid model is extended with liquid entrainment in the gas phase and gas bubbles in the liquid phase, which, according to the authors, is enough to represent the mentioned flow regimes. Bonizzi, Andreussi and Banerjee [7] showed that the model quite accurately captures the transition between flow regimes compared with a flow regime map by Taitel and Dukler [48].

The ability to capture slugs and more flow regimes is promising. However, solving the two-fluid model using an accurate discretisation can be computationally demanding. Issa and Kempf [26] used a first order upwind, staggered Finite Volume Method, which is rather diffusive compared to more advanced methods. Since too much numerical diffusion can cancel the Viscous Kelvin-Helmholtz instability, they had to use a very fine mesh. Renault [43] and Holmås [20] both came up with different solutions for an accurate and fast numerical scheme.

Renault [43] developed a slug capturing scheme based on a simplified two-fluid model and discretised it using a Lagrangian Finite Volume method. The moving mesh is used to follow slugs and fast moving waves, hence this scheme is also labelled slug tracking. The scheme is claimed to be robust and fast. Unfortunately, we could not find benchmarks supporting this. A short description of the slug tracking is given below.

The Lagrangian mesh contains elements of two different types: slugs and sections. A slug element is completely filled with liquid, for simplicity without entrainment. The liquid phase is considered to be incompressible, hence a slug moves with a uniform velocity. The velocities of the front and nose (tail) of the slug are explicitly modelled, going against the philosophy of Issa and Kempf [26], and allow the slug to grow and shrink, e.g. when the front velocity is higher than the nose velocity then the slug gains mass from the 'sections' in front and/or behind.

The section elements contain both liquid and gas in a stratified flow regime. For these elements a simplified two-fluid model is solved. Renault decoupled the momentum equations of original two-fluid equations, which makes it easier to compute, while maintaining the Viscous Kelvin-Helmholtz instability criterion of the original model needed for the correct initiation of slugs. There are in general multiple section elements between slugs, if any, and sections can be merged and split to ensure that all section elements have a similar width. An exact Riemann solver is used to resolve waves on section-section edges.

Holmås [20] studied the simulation of stratified and stratified wavy flow regimes using an incompressible two-fluid model on a fine grid. The two-fluid model is valid for long wave-

lengths, magnitudes larger than the diameter of a pipe. Short wavelengths, not resolved on a coarse mesh, are amplified by the model, which is unphysical and causes a problem when discretising the model on a fine mesh, e.g. elements widths equal to the pipe diameter. Holmås et al. [22] suggested to apply diffusion to both the mass and the momentum equation, such that the short waves are dampened. Numerical simulations confirmed the stability and showed convergence under mesh refinement.

The dissipative nature of first order discretisation methods prevents wave growth in certain situations. Holmås, Clamond and Langtangen [21] applied a pseudo-spectral Fourier method, which has exponential convergence and is hardly affected by dissipation compared to low order finite volume and finite difference methods. The space-discrete system is transformed such that the linear parts vanish, i.e. in absence of nonlinear terms the system is solved exactly. The result is integrated using a fifth-order Runge-Kutta method. According to Leebeeck and Nydal [33] the Fourier spectral method breaks down for slug flow.

The two-fluid model as used by Holmås in the first two papers, is not able to capture experimentally observed roll-waves, which do not necessarily vanish or grow and generate slugs. Holmås [19] claims that this is caused by the friction model and proposes a modified version of the Biberg friction model [6]. The Biberg friction model assumes an algebraic eddy viscosity distribution and determines the interfacial shear stress by computing the velocity profile over a cross section, approximating the pipe as a channel. The friction model is closed by relations for the amount of turbulence at the interface. Holmås improved these closure relations for roll-waves. Numerical simulations are in quite good agreement with experiments.

1.3 Improving accuracy and efficiency

Apart from Holmås [20] all numerical schemes discussed above are based on first order Finite Volume or Finite Difference Methods. A slug or flow regime capturing scheme requires a more accurate discretisation, which enlarges the computation time. For smooth hyperbolic problems it is known that the Discontinuous Galerkin Finite Element Method (DG-FEM) is computationally more efficient than the first order schemes [18]. Problems involving shocks benefit from hp-refinement: a high order basis with a coarse mesh for smooth parts and a low order basis with a fine mesh in the neighbourhood of discontinuities. We propose to use a DG-FEM method with hp-refinement to discretise a two-fluid model, which is capable of capturing flow regimes e.g. by using the friction model developed by Biberg [6].

1.4 Purpose of this report

This report is meant to give an overview of existing numerical methods for representing the multiphase flow in pipelines. The multiphase flow can contain up to three phases (gas, oil, water). The models are all time dependent and one-dimensional in space (i.e. the pipe axis). Based on the literature overview a new, more advanced numerical method will be proposed. That new model will be developed, tested, and implemented in the PhD project carried out by the author. The present report will also define some representative test cases that will be used during the course of the planned study.

1.5 Reading guide

In the following chapters we study in more detail the two-fluid model and DG-FEM discretisation. In Chapter 2 we give a brief derivation of two-fluid models, including simplifications such as assuming one or more phases to be incompressible and using a slip relation instead of a momentum balance equation. Furthermore, we discuss the modelling of friction factors.

In Chapter 3 we analyse hyperbolic problems and in particular the non-conservative subset, to which many two-fluid models belong. We give a DG-FEM weak formulation of non-conservative hyperbolic problems and discuss various methods to stabilise the weak formulation. Finally, we discuss the Runge-Kutta method for time integration of the weak formulation.

In Chapter 4 we repeat several test problems discussed in the literature. Chapter 5 concludes this report.

Chapter 2

Models

In this chapter we discuss some frequently used models for describing the flow of multiple phases in a pipeline. We start with the derivation of one-dimensional multiphase models by averaging three-dimensional conservation laws (Section 2.2). Then various assumptions and simplifications are discussed, roughly characterised as follows: using multiple pressures for the phases (Section 2.3), using a single pressure for each phase (Section 2.4), assuming the liquid phase to be incompressible (Section 2.6), using a slip relation to describe the relative velocity between the phases (Section 2.7) and assuming both phases to be incompressible and assuming a constant mixture velocity (Section 2.8). Finally, we discuss the friction terms in Section 2.9.

2.1 Notation

Let $\Omega(x,t)$ denote the cross sectional area of a pipe, not necessarily cylindrical, at position x and time t . Let a *phase* Ω_β be a subset of the pipe Ω, disjoint from other phases. We assume that the pipe is completely filled with phases, hence we may formally write

$$\cup_\beta \Omega_\beta(x,t) = \Omega(x,t), \quad \forall x,t. \tag{2.1}$$

Figure 2.1 shows an example of a pipe at some fixed point in time, containing three phases.

2.2 Averaging

As starting point for the derivation of one-dimensional multiphase models we use the general three-dimensional conservation laws for mass, momentum and energy, in Cartesian coordinates respectively given by [54]

$$\rho_{,t} + (u_j\rho)_{,j} = g^{(\rho)}, \tag{2.2}$$

$$(\rho u_i)_{,t} + (u_j\rho u_i)_{,j} = \sigma_{ij,j} + \rho g_i^{(\rho u)}, \tag{2.3}$$

$$(\rho E)_{,t} + (u_i\rho E)_{,i} = (u_i\sigma_{ij})_{,j} + (kT_{,i})_{,i} + \rho u_i g_i^{(\rho u)} + \rho g^{(\rho E)}. \tag{2.4}$$

where ρ [kg m^{-3}] is the mass density, u_i [m s^{-1}] the velocity in spatial direction i, p [Pa] the pressure, E [m^2 s^{-2}] the thermodynamic internal energy density, σ [kg m^{-1} s^{-2}] the stress tensor and $g^{(\rho)}$ [kg m^{-3} s^{-1}], $g_i^{(\rho u)}$ [m s^{-2}] and $g^{(\rho E)}$ [m^2 s^{-3}] are sources for the mass, momentum and energy equations, respectively.

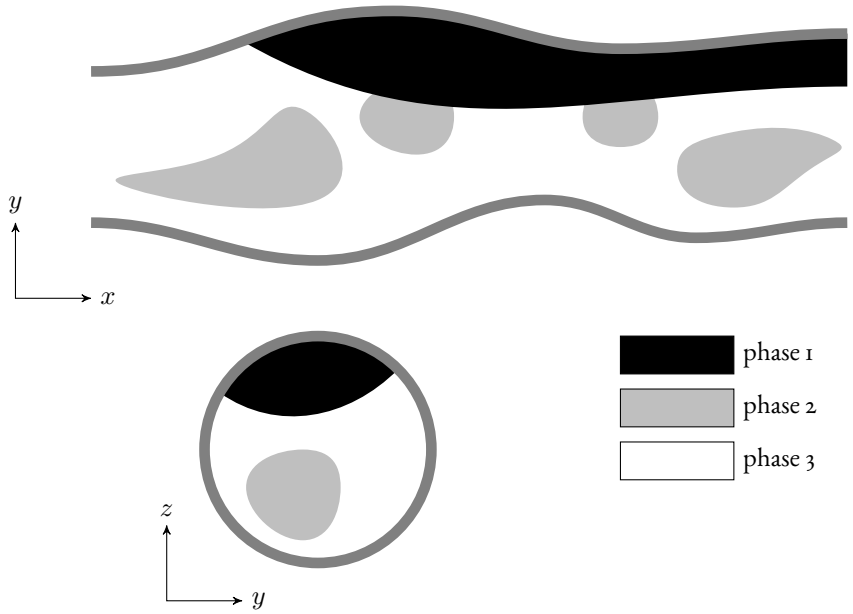

Figure 2.1: Fictitious pipe containing three immiscible phases.

Without loss of generality we may replace the stress tensor by a combination of pressure p and a viscous stress tensor τ,

$$\sigma_{ij} = -p\delta_{ij} + \tau_{ij}. \tag{2.5}$$

Some models discussed below use a different form of the energy equation (2.4), the so-called entropy equation, given by

$$T\left(\rho s\right)_{,t} + T\left(u_i \rho s\right)_{,i} = \left(E - 2e + sT - \frac{p}{\rho}\right) g^{(\rho)} + u_{i,j}\tau_{ij} + \left(kT_{,i}\right)_{,i} + \rho g^{(\rho E)}. \tag{2.6}$$

For a derivation, see Appendix A.

The three conservation laws are valid for multiphase flows. Given only these three equations, there is, however, nothing which describes the behaviour of a specific phase. The objective is to obtain a one-dimensional model which keeps track of the (one-dimensional) density of each phase. Most one-dimensional models reach this by averaging the three conservation laws over $\Omega_\beta(x,t)$, the cross section of phase β at position x and time t. We give a short derivation of a small family of one-dimensional models, following to some extent the derivations given by Ishii and Hibiki [25] and Ransom and Hicks [42].

The three conservation laws (2.2)–(2.4) can be put into the general form

$$q_{i,t} + \left(u_j q_i\right)_{,j} = f_{ij,j} + g_i, \tag{2.7}$$

where q is some conserved quantity, u a velocity and f and g may depend on q and u. Consider the integration of the first term of Equation (2.7) over cross section Ω_β. The cross section changes shape in spatial dimension x and in time t, hence interchanging integration and differentiation requires the application of Leibniz integration rule:

$$\int_{\Omega_\beta} q_{i,t} = \left(\int_{\Omega_\beta} q_i\right)_{,t} - \int_{\partial\Omega_\beta} q_i \eta_{j,t} n_j, \tag{2.8}$$

where η denotes the position of the interface as a function of time t and axial position x and n is the unit outward normal of $\partial\Omega_\beta$.

For the second term of Equation (2.7) we apply the Leibniz integration rule to the derivative to spatial dimension x and partial integration for the remaining spatial derivatives:

$$\begin{aligned}\int_{\Omega_\beta} (u_j q_i)_{,j} &= \left(\int_{\Omega_\beta} u_x q_i\right)_{,x} - \int_{\partial\Omega_\beta} u_x q_i n_j \eta_{j,x} + \int_{\partial\Omega_\beta} u_j q_i n_j \\ &= \left(\int_{\Omega_\beta} u_x q_i\right)_{,x} - \int_{\partial\Omega_\beta} q_i n_j \left(u_x \eta_{j,x} - u_j\right). \end{aligned} \tag{2.9}$$

Note that we used $n_x = 0$, which follows from Ω_β being 'flat' in the first spatial dimension, in order to write the term arising from the partial integration in a concise form. Applying Leibniz integration rule to the third term of Equation (2.7) yields

$$\int_{\Omega_\beta} f_{ij,j} = \left(\int_{\Omega_\beta} f_{ix}\right)_{,x} - \int_{\partial\Omega_\beta} \left(f_{ix} n_j \eta_{j,x} - f_{ij} n_j\right). \tag{2.10}$$

We are now ready to apply cross sectional averaging to the balance equations (2.2), (2.3), (2.4). Integration of the conservation of mass (2.2) and applying identities (2.8) and (2.9) yields

$$\left(\int_{\Omega_\beta} \rho\right)_{,t} + \left(\int_{\Omega_\beta} u_x \rho\right)_{,x} = \int_{\partial\Omega_\beta} \rho n_j \left(\eta_{j,t} + u_x \eta_{j,x} - u_j\right) + \int_{\Omega\beta} g^{(\rho)}. \tag{2.11}$$

We introduce the following shorthand notations for an average area integral

$$A_\beta q := \left(\int_\Omega 1\right)^{-1} \int_{\Omega_\beta} q, \tag{2.12}$$

and a boundary integral scaled with the cross sectional area

$$B_\beta q := \left(\int_\Omega 1\right)^{-1} \int_{\partial\Omega_\beta} q. \tag{2.13}$$

Dividing Equation (2.11) by the area of the cross section Ω, assuming the cross sectional area to be invariant in t and x and applying the shorthands yields

$$\left(A_\beta \rho\right)_{,t} + \left(A_\beta \left(u_x \rho\right)\right)_{,x} = B_\beta \left(n_j \dot{m}_j\right) + A_\beta g^{(\rho)}. \tag{2.14}$$

where

$$n_j \dot{m}_j := n_j \rho \left(\eta_{j,t} + u_x \eta_{j,x} - u_j\right). \tag{2.15}$$

The term $\dot{m}$ is the mass (per area) transfer rate through the interface $\partial\Omega_\beta$.

As we did not explicitly say anything about continuity of quantities, the velocity and density may jump at the interface. Since the interface, being infinitesimally small, cannot accumulate mass, we must ensure that, considering an interface between some phases L and G, the amount of mass flowing out of L equals the amount flowing into G and vice versa. In other words, the mass transfer rate must not jump,

$$[\![n_j \dot{m}_j]\!] = 0, \tag{2.16}$$

where n_j the normal with respect to the interface under consideration. In case there is no mass transfer at this interface, then, by Equation (2.15), the velocity in normal direction is continuous across the boundary.

We continue with the momentum balance (2.3). Application of Leibniz rules (2.8), (2.9) and (2.10) and assuming that the cross sectional area is invariant in t and x yields

$$\begin{aligned}\left(A_\beta\left(\rho u_i\right)\right)_{,t} + \left(A_\beta\left(u_x \rho u_i\right)\right)_{,x} &= B_\beta\left(n_j \dot{m}_j u_i\right) \\ &+ \left(A_\beta \sigma_{ix}\right)_{,x} - B_\beta\left(\sigma_{ix} n_j \eta_{j,x} - \sigma_{ij} n_j\right) + A_\beta\left(\rho g_i^{(\rho u)}\right). \quad (2.17)\end{aligned}$$

Doing the same for the energy balance (2.4) gives

$$\begin{aligned}\left(A_\beta\left(\rho E\right)\right)_{,t} + \left(A_\beta\left(u_x \rho E\right)\right)_{,x} &= B_\beta\left(n_j \dot{m}_j E\right) \\ &+ \left(A_\beta\left(u_i \sigma_{ix}\right)\right)_{,x} - B_\beta\left(u_i \sigma_{ix} n_j \eta_{j,x} - u_i \sigma_{ij} n_j\right) + \left(A_\beta\left(k T_{,x}\right)\right)_{,x} \\ &- B_\beta\left(k T_{,z} n_j \eta_{j,x} - k T_{,j} n_j\right) + A_\beta\left(\rho u_i g_i^{(\rho u)}\right) + A_\beta\left(\rho g^{(\rho E)}\right). \quad (2.18)\end{aligned}$$

The entropy balance (2.6) is more difficult to process. The volume integrals of the stress and temperature diffusion terms do not reduce to a boundary integral, when applying partial integration, due to the division by the temperature. Application of Leibniz rules (2.8) and (2.9) and assuming that the cross sectional area is invariant in t and x yields

$$\begin{aligned}\left(A_\beta\left(\rho s\right)\right)_{,t} + \left(A_\beta\left(u_i \rho s\right)\right)_{,x} &= B_\beta\left(n_j \dot{m}_j s\right) + A_\beta\left(\left(\frac{E}{T} - \frac{2e}{T} + s - \frac{p}{\rho T}\right) g^{(\rho)}\right) \\ &+ A_\beta\left(\frac{u_{i,j}\tau_{ij}}{T} + \frac{\left(k T_{,i}\right)_{,i}}{T}\right) + A_\beta\left(\frac{\rho g^{(\rho E)}}{T}\right). \quad (2.19)\end{aligned}$$

The averaged equations derived above are the basis for a family of one-dimensional models. Besides definitions for the sources g, the mass transfer rate $\dot{m}$ and equations of state, which are problem dependent, the model lacks closure relations for the velocity and pressure at the phase boundaries. Several simplifications of the one-dimensional balance equations (2.14), (2.17), (2.18) and (2.19) and closure relations are discusses below.

2.3 Ransom & Hicks model

One of the most complete models is formulated by Ransom and Hicks [42], amongst others. The model describes the flow of two phases in a two-dimensional channel with fixed height, assuming that one of the phases is always (completely) below the other. Furthermore, it is assumed that there is no mass transfer between phases or between a phase and the exterior of the pipe: $\dot{m} = 0$. We present a slightly more general derivation, suitable for three-dimensional pipes. First, we apply the geometry assumptions to the averaged equations derived in the previous section. Then we recall relations for the boundary values, as derived by Ransom and Hicks [42].

We generalise the geometry assumptions to three dimensions as follows. Assume the pipe has a cross section Ω, invariant in time t and axial direction x. Assume there are two phases, L and G, L being below G — think of liquid and gas — and separated at height $h : (x, t) \to \mathbb{R}$. Formally, the L and G cross sections are given by

$$\Omega_L(x,t) := \Omega \cap \{(y,z) \in \mathbb{R}^2, y < h(x,t)\}, \quad (2.20)$$

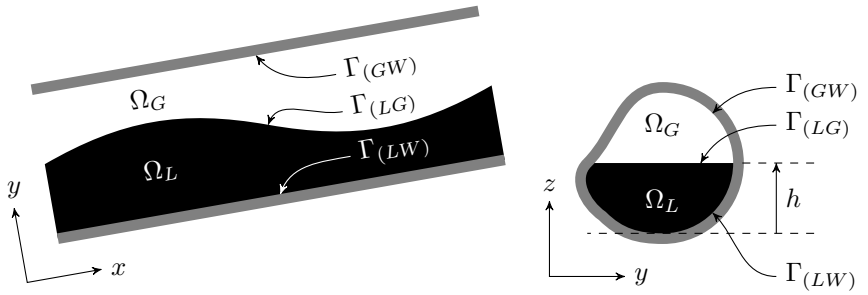

Figure 2.2: Cross section of a pipe showing the geometrical assumptions of the Ransom and Hicks model

and

$$\Omega_G(x,t) := \Omega \cap \{(y,z) \in \mathbb{R}^2, y > h(x,t)\}, \tag{2.21}$$

respectively. The position of the interface is defined by h as

$$\eta_y(x,t) := h(x,t), \tag{2.22}$$

The z-part of η is invariant in t and x. See Figure 2.2 for an example. Finally, we assume the motion in z-direction to be negligible, i.e. $u_z = 0$.

Similar to the averaging of cross sections, we apply an averaging to boundary values. Let Γ_γ denote the interface between phases L and G, phase L and the pipe wall and phase G and the pipe wall, respectively defined by

$$\Gamma_\gamma := \begin{cases} \partial\Omega_L \cap \partial\Omega_G & \text{if } \gamma = (LG), \\ \partial\Omega_L \cap \partial\Omega & \text{if } \gamma = (LW), \\ \partial\Omega_G \cap \partial\Omega & \text{if } \gamma = (GW). \end{cases} \tag{2.23}$$

The letter W in (LW) and (GW) denotes the pipe wall. Let operator $B_{\beta\gamma}$ be the boundary integral of interface $\gamma \in \{(LG), (LW), (GW)\}$ scaled by the pipe cross sectional area:

$$B_{\beta\gamma}\left(qn_j\right) := \left(\int_\Omega 1\right)^{-1} \int_{\partial\Omega_\beta \cap \Gamma_\gamma} qn_j \tag{2.24}$$

with outward normal n_j with respect to $\partial\Omega_\beta$. We approximate boundary integrals of some quantity q, e.g. u or p, by

$$B_\beta\left(qn_j\right) \approx \hat{q}_\gamma B_{\beta\gamma} n_j. \tag{2.25}$$

where $\hat{q}_\gamma : (x,t) \to \mathbb{R}$ is the average of q on Γ_γ. At the end of this section we give the relations for these average quantities as derived by Ransom and Hicks.

The averaged balance equations (2.14), (2.17) and (2.18) contain boundary integrals involving the motion of the interface. For example, the momentum equation (2.17) contains, after applying the averaging approximation (2.25), the term

$$\hat{\sigma}_{\gamma ix} B_{\beta\gamma}\left(n_j \eta_{j,x}\right). \tag{2.26}$$

By the geometry assumption, we know that the L-wall and G-wall interfaces do not change, i.e. $\eta_{,t} = \eta_{,x} = 0$ on $\Gamma_{(LW)}$ and $\Gamma_{(GW)}$. Hence

$$B_{\beta\gamma}\left(n_j \eta_{j,x}\right) = \delta_{\gamma(LG)} B_{\beta(LG)}\left(n_j \eta_{j,x}\right). \tag{2.27}$$

The remaining boundary integral can be transformed by applying Leibniz integration rule once again,

$$0 = \int_{\Omega_\beta} 1_{,x} = \left(\int_{\Omega_\beta} 1 \right)_{,x} - \int_{\Omega_\beta} \eta_{j,x} n_j. \tag{2.28}$$

This yields

$$B_{\beta\gamma} \left(n_j \eta_{j,x} \right) = \delta_{\gamma(LG)} \left(A_\beta 1 \right)_{,x}. \tag{2.29}$$

The term $A_\beta 1$ is simply the volume fraction of phase β.

We are now ready to state the set of equations defining the (three-dimensionally extended) Ransom and Hicks model. Applying the zero mass transfer assumption ($\dot{m}_j = 0$) to the mass balance equation (2.14) gives

$$\left(A_\beta \rho \right)_{,t} + \left(A_\beta \left(u_x \rho \right) \right)_{,x} = A_\beta g^{(\rho)}. \tag{2.30}$$

Applying zero mass transfer, approximation (2.25) and identity (2.29) to the averaged momentum equation (2.17) in x yields

$$\begin{aligned} \left(A_\beta \left(\rho u_x \right) \right)_{,t} + \left(A_\beta \left(u_x \rho u_x \right) \right)_{,x} &= - \left(A_\beta p \right)_{,x} + \hat{p}_{(LG)x} \left(A_\beta 1 \right)_{,x} \\ &+ \left(A_\beta \tau_{xx} \right)_{,x} - \hat{\tau}_{(LG)xx} \left(A_\beta 1 \right)_{,x} + \hat{\tau}_{\gamma x j} B_{\beta\gamma} n_j + A_\beta \left(\rho g_x^{(\rho u)} \right). \end{aligned} \tag{2.31}$$

Similarly, using the additional assumption that the velocity at the pipe wall is zero, the averaged energy equation (2.18) becomes

$$\begin{aligned} \left(A_\beta \left(\rho E \right) \right)_{,t} + \left(A_\beta \left(u_x \rho E \right) \right)_{,x} &= \left(A_\beta \left(u_i \tau_{ix} - u_x p \right) \right)_{,x} \\ - \hat{u}_{(LG)i} \hat{\tau}_{(LG)ix} \left(A_\beta 1 \right)_{,x} &+ \hat{u}_{(LG)i} \hat{\tau}_{(LG)ij} B_{\beta(LG)} n_j + \hat{u}_{(LG)x} \hat{p}_{(LG)} \left(A_\beta 1 \right)_{,x} \\ &+ \left(A_\beta \left(k T_{,x} \right) \right)_{,x} - k \hat{T}_{(LG),x} \left(A_\beta 1 \right)_{,x} + k \hat{T}_{\gamma,j} B_{\beta\gamma} n_j \\ &+ A_\beta \left(\rho u_i g_i^{(\rho u)} \right) + A_\beta \left(\rho g^{(\rho E)} \right). \end{aligned} \tag{2.32}$$

In order to write the averaged entropy equation (2.19) in this form, we need to assume that the term $u_{i,j} \tau_{ij} + \left(k T_{,i} \right)_{,i}$ vanishes, in which case the entropy equation takes the simple form

$$\begin{aligned} &\left(A_\beta \left(\rho s \right) \right)_{,t} + \left(A_\beta \left(u_x \rho s \right) \right)_{,x} \\ &\qquad = A_\beta \left(\left(\frac{E}{T} - \frac{2e}{T} + s - \frac{p}{\rho T} \right) g^{(\rho)} \right) + A_\beta \left(\frac{\rho g^{(\rho E)}}{T} \right). \end{aligned} \tag{2.33}$$

Ransom and Hicks augment the six equations (2.30), (2.31) and (2.33) for $\beta \in \{L, G\}$ with an equation describing the motion of the interface between L and G,

$$h_{,t} + \hat{u}_{(LG)x} h_{,x} = \hat{u}_{(LG)y}, \tag{2.34}$$

which is a direct result of the zero mass transfer assumption applied to Equation (2.15), and with a total vertical momentum balance, given by

$$\begin{aligned} \left(\left(A_L + A_G \right) \left(\rho u_y \right) \right)_{,t} + \left(\left(A_L + A_G \right) \left(u_x \rho u_y \right) \right)_{,x} &= - \hat{p}_{(LW)} B_{L(LW)} n_y - \hat{p}_{(GW)} B_{G(GW)} n_y \\ + \left(\left(A_L + A_G \right) \tau_{yx} \right)_{,x} + \hat{\tau}_{(LW)yj} B_{L(LW)} n_j &+ \hat{\tau}_{(GW)yj} B_{G(GW)} n_j \\ &+ \left(A_L + A_G \right) \left(\rho g_y^{(\rho u)} \right), \end{aligned} \tag{2.35}$$

which follows from summing the averaged momentum balance (2.17) for both phases L and G.

We now apply a series of approximations to the eight differential equations in order to reduce the number of unknowns. The averages of products are approximated by products of averages, e.g.

$$A_\beta \left(\rho u_i\right) \approx \overline{\rho}_\beta \overline{u}_{\beta i} A_\beta 1, \tag{2.36}$$

(no Einstein summation!). Furthermore, the following interface terms are approximated. For a justification we refer the reader to Ransom and Hicks [42]. The mass-weighted average transverse velocity is approximated by the transverse velocity at the interface between L and G:

$$\frac{\left(A_L + A_G\right)\left(\rho u_y\right)}{\left(A_L + A_G\right)\rho} \approx \hat{u}_{(LG)y} \tag{2.37}$$

The axial velocity at the interface between L and G is approximated by a equal-weighted average of the average axial phase velocities:

$$\hat{u}_{(LG)x} \approx \tfrac{1}{2}\left(\overline{u}_{Lx} + \overline{u}_{Gx}\right). \tag{2.38}$$

The pressure terms at the three interfaces are approximated as follows:

$$\hat{p}_{(LW)} \approx \overline{p}_L, \tag{2.39}$$

$$\hat{p}_{(GW)} \approx \overline{p}_G, \tag{2.40}$$

and

$$\hat{p}_{(LG)} \approx \tfrac{1}{2}\left(\overline{p}_L + \overline{p}_G\right). \tag{2.41}$$

This completes the model up to equations of state, a viscous stress tensor τ_{ij} and a relation between the height of the interface h and the volume fractions $A_\beta 1$. The viscous stress tensor will be discussed in Section 2.9.

Above approximations lead to a hyperbolic one-dimensional model, as proven by Ransom and Hicks [42]. The model is, however, not conservative, even if we ignore the sources g and the viscous stress tensor τ: see Equations (2.31) and (2.34).

2.3.1 Transverse hydrodynamic behaviour

The two pressure models by Ransom and Hicks [42] explicitly model hydrodynamic behaviour in transversal direction. Or, to be more precise, other models explicitly remove hydrodynamic behaviour by assuming a hydrostatic situation in transversal direction, with or without a gravity.

To analyse the transverse dynamic behaviour of the model we consider a channel (2D) with height H [m], ignore all variation in x and assume both phases to be inviscid. Furthermore, we assume all sources, including mass transfer, to be zero. The model reduces to the following set of equations.

$$\left(A_\beta \rho\right)_{,t} = 0, \quad \beta \in \{L, G\} \tag{2.42}$$

$$\left(A_\beta \left(u_x \rho\right)\right)_{,t} = 0, \quad \beta \in \{L, G\} \tag{2.43}$$

$$\left(A_\beta \left(\rho s\right)\right)_{,t} = 0, \quad \beta \in \{L, G\} \tag{2.44}$$

$$h_{,t} = \hat{u}_{(LG)y}, \tag{2.45}$$

$$\left(\left(A_L \rho + A_G \rho\right)\hat{u}_{(LG)y}\right)_{,t} = \overline{p}_L - \overline{p}_G. \tag{2.46}$$

By Equation (2.42), the total density per phase $A_\beta \rho$ does not change in time. Let the mixture density ρ_m be defined by

$$\rho_m := (A_L + A_G)\,\rho. \tag{2.47}$$

Then, the mixture transverse momentum equation (2.46) becomes

$$\rho_m \hat{u}_{(LG)y,t} = \overline{p}_L - \overline{p}_G. \tag{2.48}$$

Combining this equation with equation (2.45) gives the following ordinary differential equation describing the height of the interface between L and G:

$$h_{,tt} = \frac{1}{\rho_m}\left(\overline{p}_L - \overline{p}_G\right). \tag{2.49}$$

Since we assume a two-dimensional system, the relation between the height h and the volume fractions is simply given by:

$$HA_L 1 = h, \tag{2.50}$$

and

$$HA_G 1 = H - h. \tag{2.51}$$

The average density per phase $\overline{\rho}_\beta$ is then found by dividing the averaged phase density by the volume fraction:

$$\overline{\rho}_L = \frac{HA_L\rho}{h}, \tag{2.52}$$

and

$$\overline{\rho}_G = \frac{HA_G\rho}{H-h}. \tag{2.53}$$

We assume the following equations of state. Phase G satisfies the ideal gas law:

$$\overline{p}_G = \overline{\rho}_G c_G^2. \tag{2.54}$$

where c_L is the speed of sound of phase L. For phase L we use a linear relation around a point determined by density ρ_{0L} and pressure p_{0L}:

$$\overline{p}_L = \left(\overline{\rho}_L - \rho_{0L}\right) c_L^2 + p_{0L}, \tag{2.55}$$

here, c_L is the speed of sound of phase L.

Substituting equations (2.50)–(2.55) in equation (2.49) gives the ODE

$$h_{,tt} = \frac{1}{\rho_m}\left(\frac{HA_L\rho c_L^2}{h} - \rho_{0L}c_L^2 + p_{0L} - \frac{HA_G\rho c_G^2}{H-h}\right). \tag{2.56}$$

We will derive a solution to a linearisation of this ODE around the equilibrium point h_0. To find h_0 we need to solve the following equation:

$$0 = \frac{HA_L\rho c_L^2}{h_0} - \rho_{0L}c_L^2 + p_{0L} - \frac{HA_G\rho c_G^2}{H-h_0}. \tag{2.57}$$

Multiplying with $h_0 \left(H - h_0\right)$ gives the quadratic equation

$$\begin{aligned} 0 = {} & h_0^2 \left(\rho_{0L} c_L^2 - p_{0L}\right) \\ & + h_0 \left(-H\rho_{0L} c_L^2 + H p_{0L} - H A_L \rho c_L^2 - H A_G \rho c_G^2\right) + H^2 A_L \rho c_L^2. \end{aligned} \tag{2.58}$$

The physical solution should should satisfy $0 \leq h_0 \leq H$. Note that under certain circumstances there might be no physical solutions h_0.

Linearising the ODE (2.56) around the equilibrium point gives

$$h_{,tt} = -\omega^2 \left(h - h_0\right), \tag{2.59}$$

where ω is given by

$$\omega = \sqrt{\frac{1}{\rho_m} \left(\frac{H A_L \rho c_L^2}{h_0^2} + \frac{H A_G \rho c_G^2}{\left(H - h_0\right)^2} \right)}. \tag{2.60}$$

The solution of the ODE is given by

$$h = h_0 + k_1 \cos \omega t + k_2 \sin \omega t, \tag{2.61}$$

where $k_1, k_2 \in \mathbb{R}$ are coefficients independent of t.

Consider the following situation:

$$H = 1\,\mathrm{m}, \tag{2.62}$$
$$h_0 = 0.25\,\mathrm{m}, \tag{2.63}$$
$$p_0 = 10^5\,\mathrm{Pa}, \tag{2.64}$$
$$p_{0L} = 10^5\,\mathrm{Pa}, \tag{2.65}$$
$$\rho_{0L} = 1000\,\mathrm{kg\,m^{-3}}, \tag{2.66}$$
$$c_L = 1500\,\mathrm{m\,s^{-1}}, \tag{2.67}$$
$$c_G = 300\,\mathrm{m\,s^{-1}}. \tag{2.68}$$

In this case we choose an equilibrium height h_0 and pressure p_0 and let the constants $A_L \rho$ and $A_G \rho$ be derived from these quantities. This situation is roughly equivalent to a pipe filled with one quarter of water and three quarters of air, both phases being at room temperature and one bar. Using equation (2.60) we can compute the oscillation frequency of the system:

$$\omega \approx 6 \cdot 10^3\,\mathrm{s^{-1}}. \tag{2.69}$$

If we advance the system with a classical fourth order, explicit Runge-Kutta method, then the restriction on the time step is

$$\Delta t \lessapprox 5 \cdot 10^{-4}\,\mathrm{s}. \tag{2.70}$$

To put this into perspective, we compute the time step restriction based on a first order Finite Volume discretisation, ignoring source terms, and a fourth order, explicit Runge-Kutta method time integration. The largest eigenvalue of the hyperbolic model is roughly equal to the speed of sound of phase L. This gives the CFL condition [11]

$$\frac{c_L \Delta T}{\Delta x} \leq 1.392, \tag{2.71}$$

which is comparable to restriction (2.70) when $\Delta x \approx 0.54\,\mathrm{m}$. For the simulation of very long pipelines, much wider elements are used in practice, in which case the restriction due to the source terms (2.70) is dominant.

2.4 Equal pressure

As discussed previously, the transverse momentum equation (2.35) as used in the Ransom and Hicks model may have a very small time scale, compared to the other differential equations. This might pose a problem when discretising these equations. In many models the transverse momentum equations are ignored and it is assumed that at every axial point of the pipe the pressure is constant in y and z:

$$p(x, y, z, t) = \overline{p}(x, t). \tag{2.72}$$

Applying this assumption to the averaged momentum equations (2.17) yields

$$\begin{aligned}\left(A_\beta\left(\rho u_x\right)\right)_{,t} + \left(A_\beta\left(u_x \rho u_x\right)\right)_{,x} + \overline{p}_{,x} A_\beta 1 \\ = B_\beta\left(n_j \dot{m}_j u_x\right) + A_\beta\left(\tau_{xx} n_j v_j^{(x)} - \tau_{xj} n_j\right) + A_\beta\left(\rho g_x^{(\rho u)}\right).\end{aligned} \tag{2.73}$$

Note that we do not assume a certain geometry of the phases, contrary to the Ransom and Hicks model. Together with the mass balance (2.14), approximation (2.36), equations of state and a relation for the viscous stress tensor, this forms a complete model. This model features only three differential equations per phase, whereas the Ransom and Hicks model consists of eight equations for two phases. Both models are non-conservative.

A consequence of the equal pressure assumption is that the model is not unconditionally hyperbolic. In the case of a system with two phases, say L and G, Stewart and Wendroff [47] showed that the model is *not* hyperbolic if the following condition holds:

$$0 < \left(\overline{u}_{Gx} - \overline{u}_{Lx}\right)^2 < \frac{a_L^2 a_G^2}{\alpha_L \rho_G a_G^2 + \alpha_G \rho_L a_L^2}\left(\left(\alpha_G \rho_L\right)^{\frac{1}{3}} + \left(\alpha_L \rho_G\right)^{\frac{1}{3}}\right)^3. \tag{2.74}$$

When the phase velocities are close to each other, which can occur in practice, the model becomes non-hyperbolic. Several solutions have been proposed in the literature to (re)gain unconditional hyperbolicity, based on a different choice for the pressure at the interface between the two phases. Re-deriving the momentum equation with the assumption that the average pressure per phase equals $\overline{p}$ yields

$$\begin{aligned}\left(A_\beta\left(\rho u_x\right)\right)_{,t} + \left(A_\beta\left(u_x \rho u_x\right)\right)_{,x} = -\left(A_\beta \overline{p}\right)_{,x} + \hat{p}_{(LG)}\left(A_\beta 1\right)_{,x} \\ + \left(A_\beta \tau_{xx}\right)_{,x} - \hat{\tau}_{(LG)xx}\left(A_\beta 1\right)_{,x} + \hat{\tau}_{\gamma x j} B_{\beta\gamma} n_j + A_\beta\left(\rho g_x^{(\rho u)}\right).\end{aligned} \tag{2.75}$$

In CATHARE [5] (with $\delta = 1$) and in Evje and Flåtten [14] (with $\delta = 1.2$) the pressure at the interface is chosen such that the system is unconditionally hyperbolic:

$$\overline{p} - \hat{p}_{(LG)} = \delta \frac{\alpha_L \alpha_G \overline{\rho}_L \overline{\rho}_G}{\alpha_L \overline{\rho}_G + \alpha_G \overline{\rho}_L}\left(\overline{u}_L - \overline{u}_G\right)^2. \tag{2.76}$$

Choosing $\delta \geq 1$ ensures hyperbolicity [14]. Toumi, Kumbaro and Paillere [51] discuss several other choices for the pressure at the interface.

2.5 Hydrostatic pressure

The pressure of a fluid varies e.g. in y under influence of gravity. We can take vertical pressure variation due to gravity into account by solving the momentum balance equation (2.3) in

direction y assuming the fluid is in equilibrium, i.e. $(\rho u_i)_{,t} = u_y = 0$, and the source term $g_y^{(\rho u)} = g_{\text{grav}} \cos\theta$, g_{grav} being the accelaration due to gravity. This gives

$$p_{,y}(y) = -\rho(y)\, g_{\text{grav}} \cos\theta. \tag{2.77}$$

Please note that the the x-direction follows the pipe, while y is perpendicular to the pipe wall, hence the term $\cos\theta$ in the gravity force. Solving this equation analytically for a particular phase β can be difficult, depending on the equation of state. We assume, however, that the density variation is negligible and replace $\rho(y)$ with the density at a reference point y_{ref}. Furthermore, we assume that the phase lives in a section $\Omega_\beta = \{(y,z) \in \Omega \,:\, h \leq y \leq h\}$. This yields

$$p_{,y}(y) = -\rho(y_{\text{ref}})\, g_{\text{grav}} \cos\theta, \quad h < y < h, \tag{2.78}$$

where $h < y_{\text{ref}} < h$. Solving this simplified equation for p gives

$$p(y) = p(y_{\text{ref}}) - (y - y_{\text{ref}})\, \rho(y_{\text{ref}})\, g_{\text{grav}} \cos\theta, \quad h < y < h, \tag{2.79}$$

where $p(y_{\text{ref}})$ and $\rho(y_{\text{ref}})$ are related via the equation of state. If we choose y_{ref} such that

$$y_{\text{ref}} A_\beta 1 = A_\beta y, \tag{2.80}$$

then $p(y_{\text{ref}})$ is the average pressure of the phase. Finally, imposing continuity of the pressure gives a set of $n-1$ relations for the (average) phase pressures, where n is the number of phases.

An example using two phases L and G. Let h be the height of the interface between L and G and H the height of the pipe. The pressure in phase L is given by

$$p(y) = \overline{p}_L - (y - y_{\text{ref};L})\, \overline{\rho}_L g_{\text{grav}} \cos\theta, \quad 0 \leq y < h, \tag{2.81}$$

and the pressure in phase G by

$$p(y) = \overline{p}_G - (y - y_{\text{ref};G})\, \overline{\rho}_G g_{\text{grav}} \cos\theta, \quad h < y \leq H. \tag{2.82}$$

Imposing continuity at h, ignoring surface tension, gives a relation between the average pressure of both phases,

$$p(h) := \lim_{y \nearrow h} p(y) = \lim_{y \searrow h} p(y). \tag{2.83}$$

The pressure at the interface including the pressure correction term as discussed in the previous section is given by

$$p(h) - \hat{p}_{(LG)} = \delta \frac{\alpha_L \alpha_G \overline{\rho}_L \overline{\rho}_G}{\alpha_L \overline{\rho}_G + \alpha_G \overline{\rho}_L} \left(\overline{u}_L - \overline{u}_G\right)^2. \tag{2.84}$$

These definitions of pressure and interface presure can be used in the following momentum balance equation,

$$\begin{aligned}\left(A_\beta (\rho u_x)\right)_{,t} + \left(A_\beta (u_x \rho u_x)\right)_{,x} &= -\left(A_\beta p\right)_{,x} + \hat{p}_{(LG)} \left(A_\beta 1\right)_{,x} \\ &+ \left(A_\beta \tau_{xx}\right)_{,x} - \hat{\tau}_{(LG)xx} \left(A_\beta 1\right)_{,x} + \hat{\tau}_{\gamma x j} B_{\beta\gamma} n_j + A_\beta \left(\rho g_x^{(\rho u)}\right).\end{aligned} \tag{2.85}$$

Henkes, Vreenegoor and Haandrikman [17] use a slightly different, but analytically identical form of the momentum balance equation with $\delta = 0$, where the term $A_\beta p$ is replaced by terms involving the interface pressure $p(h)$. In fact the formulation of Henkes et al. is

used in most of the industrial pipeline tools, like OLGA, LedaFlow, and Compas. We show, in two different ways, the equivalence with (2.85) in case of two phases.

We choose the reference point y_{ref} at the interface, $y_{\text{ref}} = h$, and substitute the hydrostatic pressure equation (2.79) in the term $(A_\beta p)_{,x}$. This gives

$$(A_\beta p)_{,x} = \left(A_\beta \left(p(h) - (y-h)\,\overline{\rho} g_{\text{grav}} \cos\theta\right)\right)_{,x} \tag{2.86}$$

$$= (A_\beta)_{,x}\, p(h) + A_\beta p_{,x}(h) - \left(A_\beta \left((y-h)\,\overline{\rho} g_{\text{grav}} \cos\theta\right)\right)_{,x}. \tag{2.87}$$

Applying the Leibniz integration rule (2.8) with t replaced by x yields

$$\left(A_\beta \left((y-h)\,\overline{\rho} g_{\text{grav}} \cos\theta\right)\right)_{,x} = A_\beta \left(h_{,x} \overline{\rho} g_{\text{grav}} \cos\theta\right) - B_\beta \left((y-h)\,\overline{\rho} g_{\text{grav}} \cos\theta \eta_{j,x} n_j\right) \tag{2.88}$$

$$= A_\beta \left(h_{,x} \overline{\rho} g_{\text{grav}} \cos\theta\right). \tag{2.89}$$

The boundary integral vanishes because $y - h = 0$ at the interface and $\eta_{j,x} = 0$ at the pipe wall, assuming that the pipe does not change the geometry in x. Finally, the two pressure terms in the momentum equation (2.85) become

$$(A_\beta p)_{,x} - \hat{p}_{(LG)} (A_\beta 1)_{,x} = A_\beta (p_{,x}(h)) + A_\beta \left(h_{,x} \overline{\rho} g_{\text{grav}} \cos\theta\right) + \left(p(h) - \hat{p}_{(LG)}\right) (A_\beta)_{,x}. \tag{2.90}$$

For the second derivation we start with the pressure as defined by equations (2.81) and (2.82), which defines the reference points $y_{\text{ref};L}$ and $y_{\text{ref};G}$ such that $A_L p = p(y_{\text{ref};L})\, A_L 1$ and $A_G p = p(y_{\text{ref};G})\, A_G 1$. We start with the liquid phase. Substituting Equation (2.81) in $A_L p$ gives

$$A_L p = \overline{p}_L A_L 1 = p(h)\, A_L 1 + (h - y_{\text{ref};L})\, \overline{\rho}_L g_{\text{grav}} \cos\theta A_L 1 \tag{2.91}$$

$$= p(h)\, A_L 1 + \overline{\rho}_L g_{\text{grav}} \cos\theta A_L (h - y). \tag{2.92}$$

where we used the identity (2.80). Taking the derivative of $A_L p$ to x gives

$$(A_L p)_{,x} = p_{,x}(h)\, A_L 1 + p(h)\, (A_L 1)_{,x} + \overline{\rho}_L g_{\text{grav}} \cos\theta \left(A_L (h-y)\right)_{,x} \tag{2.93}$$

$$= p_{,x}(h)\, A_L 1 + p(h)\, (A_L 1)_{,x} + \overline{\rho}_L g_{\text{grav}} \cos\theta \left(A_L h_{,x} + B_L \left((h-y)\,\eta_{j,x} n_j\right)\right). \tag{2.94}$$

The boundary integral vanishes because $y - h = 0$ at the interface and $\eta_{j,x} = 0$ at the pipe wall, assuming that the pipe does not change the geometry in x, hence

$$\begin{aligned}(A_L p)_{,x} &= p_{,x}(h)\, A_L 1 + p(h)\, (A_L 1)_{,x} \\ &= p_{,x}(h)\, A_L 1 + p(h)\, (A_L 1)_{,x} + \overline{\rho}_L g_{\text{grav}} \cos\theta A_L h_{,x}.\end{aligned} \tag{2.95}$$

Finally, the two pressure terms in the momentum equation (2.85) become

$$(A_L p)_{,x} - \hat{p}_{(LG)} (A_L 1)_{,x} = p_{,x}(h)\, A_L 1 + \left(p(h) - \hat{p}_{(LG)}\right) (A_L 1)_{,x} + h_{,x} \overline{\rho}_L g_{\text{grav}} \cos\theta A_L 1. \tag{2.96}$$

For the gas phase the analysis is exactly the same:

$$(A_G p)_{,x} - \hat{p}_{(LG)} (A_G 1)_{,x} = p_{,x}(h)\, A_G 1 + \left(p(h) - \hat{p}_{(LG)}\right) (A_G 1)_{,x} + h_{,x} \overline{\rho}_G g_{\text{grav}} \cos\theta A_G 1. \tag{2.97}$$

The terms with $h_{,x}$ in equations (2.96) and (2.96) are also referred to as the 'hydraulic gradients'. They enable (depending on the precise conditions) the initiation and growth of unstable waves and slugs starting with a stratified base flow.

2.6 Incompressible phase

Under some circumstances we may assume that one of the phases, say a liquid phase, is incompressible. This implies that the density of the respective phase is constant. The general averaged equations (2.14), (2.17) and (2.18) remain valid. In case of a two phase, (y,z-invariant pressure) hydrostatic equilibrium model, discussed in the previous section, we may exploit the incompressibility to obtain a set of conservative equations. [50]

Let subscript L denote an incompressible phase. Approximating averages of products with products of averages, see Equation (2.36), gives the following averaged axial momentum equation:

$$\begin{aligned}\left(\alpha_L\overline{\rho}_L\overline{u}_{Lx}\right)_{,t} + \left(\alpha_L\overline{\rho}_L\overline{u}_{Lx}^2\right)_{,x} + \alpha_L p_{,x} = B_L\left(n_j\dot{m}_j u_x\right) \\ + \left(A_L\tau_{xx}\right)_{,x} - B_L\left(\tau_{xx}n_j\eta_{j,x} - \tau_{xj}n_j\right) + A_L\left(\rho g_x^{(\rho u)}\right). \quad (2.98)\end{aligned}$$

Substituting mass balance equation (2.14) and approximating boundary term $B_L\left(n_j\dot{m}_j u_x\right)$ with $B_L\left(n_j\dot{m}_j\right)\overline{u}_{Lx}$ yields

$$\begin{aligned}\alpha_L\overline{\rho}_L\overline{u}_{Lx,t} + \frac{1}{2}\alpha_L\overline{\rho}_L\overline{u}_{Lx,x}^2 + \overline{u}_L A_L g^{(\rho)} + \alpha_L p_{,x} \\ = \left(A_L\tau_{xx}\right)_{,x} - B_L\left(\tau_{xx}n_j\eta_{j,x} - \tau_{xj}n_j\right) + A_L\left(\rho g_x^{(\rho u)}\right). \quad (2.99)\end{aligned}$$

Dividing by $\alpha_L\overline{\rho}_L$ yields an equation without non-conservative products, that is, when we ignore the terms involving the viscous stress tensor τ.

The averaged axial momentum equation for the remaining compressible phase (2.73) is non-conservative. Instead, we use the sum of momentum equations for both phases, which *is* conservative:

$$\begin{aligned}\sum_\beta\left(A_\beta\left(\rho u\right)\right)_{,t} + \sum_\beta\left(A_\beta\left(u_x\rho u_x\right)\right)_{,x} + \sum_\beta\left(A_\beta p\right)_{,x} = \sum_\beta B_\beta\left(n_j\dot{m}_j u_x\right) \\ + \sum_\beta\left(A_\beta\tau_{xx}\right)_{,x} + \sum_\beta B_\beta\left(\tau_{xx}n_j\eta_{j,x} - \tau_{xj}n_j\right) + \sum_\beta A_\beta\left(\rho g_x^{(\rho u)}\right). \quad (2.100)\end{aligned}$$

If the cross section of the pipe Ω is invariant in x, then a part of the boundary integral involving τ vanishes:

$$\sum_\beta B_\beta\left(\tau_{xx}n_j\eta_{j,x}\right) = 0. \quad (2.101)$$

Together with the mass balance (2.14), the energy balance (2.18) and an equation of state for the compressible phase, this forms a conservative model up to the terms involving mass transfer and viscous stress tensor.

2.7 Slip relation

When a strong coupling exists between two phases, it suffices to use a mixture momentum equation (2.100) and a so-called slip relation describing the relative motion of the phases.

Zuber and Findlay [56] derived a general slip relation suitable for any flow regime involving two phases:

$$\overline{u}_G = C_0\delta_\beta A_\beta u + \frac{A_G u_r}{A_G 1} \quad (2.102)$$

Here, C_0 is a phase distribution parameter: < 1 if the gas concentration is higher at the center than close to the pipe wall and > 1 if the gas concentration is higher close to the pipe wall. For the second term several definitions are given for different flow regimes. For example for slug flow the following definition may be used,

$$\frac{A_G u_r}{A_g} = 0.35 \left(\frac{f_{\text{gravity}} \left(\overline{\rho}_L - \overline{\rho}_G \right) D}{\rho_1} \right)^{\frac{1}{2}}. \tag{2.103}$$

and for churn-turbulent bubbly flow,

$$\frac{A_G u_r}{A_g} = 1.53 \left(\frac{\sigma f_{\text{gravity}} \left(\overline{\rho}_L - \overline{\rho}_G \right)}{\rho_L} \right)^{\frac{1}{4}}, \tag{2.104}$$

where D [m] denotes the diameter of the pipe and σ [m s^{-2}] the surface tension.

2.8 Incompressible phases with constant mixture velocity

Wangensteen [53] studied an isentropic two-phase model with the assumptions that both phases are incompressible and the mixture velocity is constant. The model consists of just two PDE's. The derivation is as follows.

Dividing the mass balance (2.14) by the constant density ρ and ignoring sources and mass transfer gives

$$\left(A_\beta 1 \right)_{,t} + \left(A_\beta u_x \right)_{,x} = 0. \tag{2.105}$$

We define the mixture velocity u_m as

$$u_m := \sum_\beta A_\beta u_x. \tag{2.106}$$

Given the mixture velocity, we need one more equation in order to find both phase velocities. Since we have no information about the pressure we choose a linear combination of the equal pressure momentum balance equations (2.73) such that the pressure term vanishes:

$$\begin{aligned} &\left(A_{L-G} \left(\rho u_i \right) \right)_{,t} + \left(A_{L-G} \left(u_x \rho u_i \right) \right)_{,x} = \\ &\qquad \left(A_{L-G} \tau_{ix} \right)_{,x} - B_{L-G} \left(\tau_{ix} n_j \eta_{j,x} - \tau_{ij} n_j \right) + A_{L-G} \left(\rho g_i^{(\rho u)} \right). \end{aligned} \tag{2.107}$$

where $A_{L-G} f := A_G 1 A_L f - A_L 1 A_G f$ and $B_{L-G} = A_G 1 B_L f - A_L 1 B_G f$.

Any linear combination of the volume fraction balance (2.105), the volume equation ($\sum_\beta A_\beta 1 = 1$), the momentum difference equation (2.107) and some relation for the mixture velocity (2.106) gives a complete model.

2.9 Flow regimes

Besides averaged quantities, the models described above depend on quantities at boundaries, such as the mass transfer rate $\dot{m}$ and the viscous stress tensor τ. Especially the viscous stress and the size of the (cross sectional) phase boundary depend on the shape of the (cross sectional) phase.

In order to find these boundary values, we need to determine the so-called flow regime. There are various flow regimes distinguished by different authors. Here, we give a couple

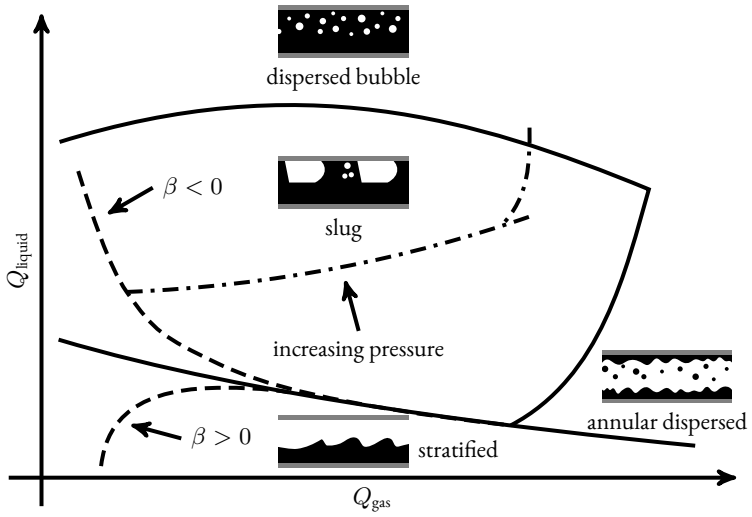

Figure 2.3: Flow pattern map from [30] (reillustrated)

of examples. A flow regime where multiple phases are separated in height is called *stratified flow*. This is used in the Ransom and Hicks model, discussed in Section 2.3. Some authors distinguish a *smooth* and a *wavy* version. In case there is an outer layer of liquid and an inner core of gas the flow regime is called *annular*. In case there are liquid droplets transported in the gas phase, it is called *annular dispersed*. A flow pattern map can be used to determine the flow regime based on the mass flow rates. Figure 2.3 shows an example flow pattern map. See also Taitel and Dukler [48] for a discussion about flow regimes and transitions.

In the remainder of this section we focus on the stratified flow regime. Based on this flow regime we want to derive a relation between average phase velocities and viscous stresses at the phase boundaries. First consider a single phase situation. Note that the averaged equations (2.14), (2.17) and (2.18) remain valid in this special case. Poiseuille obtained experimentally a relation for the pressure drop for viscous, incompressible, laminar flows in a smooth, cylindrical pipe, involving a function/constant depending on the temperature and the type of fluid, later recognised as the viscosity. Later the following equation is derived, in accordance with Poiseuille's result, based on the Navier-Stokes equations and the no-slip boundary condition,

$$p_{,x} = \frac{8\mu\overline{u}_x}{r^2}, \tag{2.108}$$

called the Hagen-Poiseuille law/equation, although usually stated in terms of head loss instead of pressure drop. Here, $\overline{u}_x$ $[\mathrm{m\,s^{-1}}]$ denotes the average velocity of the flow and r $[\mathrm{m}]$ the pipe radius.

For high/higher Reynolds numbers, the flow becomes turbulent with a laminar boundary layer. The size of the boundary layer decreases with increasing Reynolds number, until the size becomes comparable with the roughness of the wall, in which case the laminar layer breaks up completely and the flow becomes fully turbulent [37]. Due to the turbulence the Hagen-Poiseuille equation fails to hold. Instead, the Darcy formula can be used to determine the pressure drop,

$$p_{,x} = \frac{f_D\rho|\overline{u}_x|\overline{u}_x}{4r}, \tag{2.109}$$

where f_D denotes the Darcy friction factor. The friction factor depends on the Reynolds

number of the flow, usually defined as

$$Re = \frac{2r\rho|\overline{u}_x|}{\mu}, \tag{2.110}$$

and the ratio of the pipe roughness, ϵ [m], and pipe diameter.

For completely turbulent flow, von Kármán [29] derived the following Darcy friction factor

$$f_{D,\text{turbulent}} := \left(1.74 + 2\log\frac{r}{\epsilon}\right)^{-2}. \tag{2.111}$$

For completely laminar flow, the Darcy friction factor follows from the Hagen-Poiseuille equation (2.108),

$$f_{D,\text{laminar}} := \frac{64}{Re}. \tag{2.112}$$

For intermediate Reynolds numbers, the Colebrook function may be used to approximate the friction factor. The Colebrook relation was conveniently drawn in a chart by Moody [37].

Applying the Darcy formula (2.109) and incompressibility and steady state assumptions to the averaged equations (2.14), (2.17) and (2.18) yields the following equalities for the viscous stress terms,

$$B_Y\left(\tau_{ij}n_j\right) = \frac{f_{D;Y}\rho_Y|\overline{u}_{Yx}|\overline{u}_{Yx}}{4r}, \tag{2.113}$$

$$B_Y\left(\tau_{ix}n_j v_j^{(x)}\right) = 0. \tag{2.114}$$

$$\left(A_Y\tau_{ix}\right)_{,x} = 0, \tag{2.115}$$

Where the last equality follows from (also) assuming the fluid to be Newtonian. Due to symmetry we may write the normal component of the viscous stress as

$$\tau_{ij}n_j = \tfrac{1}{8}f_{D;Y}\rho_Y|\overline{u}_{Yx}|\overline{u}_{Yx}. \tag{2.116}$$

The above discussion holds for single phase flow in cylindrical pipes. In case of two phases, say liquid and gas, respectively denoted by L and G, equality (2.116) is commonly used to approximate the viscous terms, yielding

$$B_{L(LW)}\left(\tau_{ij}n_j\right) \approx \tfrac{1}{8}f_{D;L(LW)}\rho_L|\overline{u}_{Lx}|\overline{u}_{Lx}B_{L(LW)}1, \tag{2.117}$$

and

$$B_{G(GW)}\left(\tau_{ij}n_j\right) \approx \tfrac{1}{8}f_{D;G(GW)}\rho_G|\overline{u}_{Gx}|\overline{u}_{Gx}B_{G(GW)}1, \tag{2.118}$$

for the liquid-wall and gas-wall interface, respectively. The friction at the interface between the gas and the liquid phase is approximated by

$$B_{G(GL)}\left(\tau_{ij}n_j\right) \approx \tfrac{1}{8}f_{D;G(GL)}\rho_G|\overline{u}_{Gx} - \overline{u}_{Lx}|\left(\overline{u}_{Gx} - \overline{u}_{Lx}\right)B_{G(GL)}1. \tag{2.119}$$

By conservation of momentum:

$$B_{L(LG)}\left(\tau_{ij}n_j\right) \approx -B_{G(GL)}\left(\tau_{ij}n_j\right). \tag{2.120}$$

Chapter 3

Discretisation

The models discussed in Chapter 2 are (conditionally) hyperbolic. In this chapter we discuss various discretisation methods for this type of differential equations. In the second section we discuss properties of hyperbolic systems, such as uniqueness, and the so-called Riemann problem, which is extensively used in discretisations. In Section 3.3 we discuss a DG-FEM weak formulation for non-conservative systems. In Section 3.4 we give a stabilisation method for the weak formulation. In Section 3.5 we discuss a method for reducing oscillations in high-order discretisation. Finally, in Section 3.6 the Runge-Kutta method for time integration is discussed.

In Appendix B we give some background information on the DG-FEM.

3.1 Notation

Let $\Omega \subset \mathbb{R}$ and $f : \Omega \to \mathbb{C}^n$ any function. Then the jump of f on $x \in \Omega$ is defined by

$$[\![f]\!](x) := \lim_{y \searrow x} f(x) - \lim_{y \nearrow x} f(x), \tag{3.1}$$

and the average value of f at x by

$$\{\!\{f\}\!\}(x) := \frac{\lim_{y \searrow x} f(x) + \lim_{y \nearrow x} f(x)}{2}. \tag{3.2}$$

Note that if f is continuous at x, then $[\![f]\!](x) = 0$ and $\{\!\{f\}\!\}(x) = f(x)$.

Let $f, g : \Omega \to \mathbb{R}^n$ with $\Omega \subset \mathbb{R}$. Then the following relation holds,

$$[\![fg]\!] = \{\!\{f\}\!\} [\![g]\!] + [\![f]\!] \{\!\{g\}\!\}. \tag{3.3}$$

3.2 Properties of hyperbolic systems

Consider a system of n partial differential equations in time t and space dimension x given by

$$u_{i,t}(x,t) + g_{ij}(u(x,t), x, t)\, u_{j,x}(x,t) = 0 \quad \text{for almost all } x \in X, t \in T, \tag{3.4}$$

where the solution $u : X \times T \to \mathbb{R}^n$ is a function of space and time and $g : \mathbb{R}^n \times X \times T \to \mathbb{R}^{n \times n}$ is a matrix dependent on the solution u, space and time and subsets $X, T \subset \mathbb{R}$ define the space and time domain, respectively.

Definition 3.1 (hyperbolicity). Let $n \in \mathbb{N}$, $g : \mathbb{R}^n \times X \times T \to \mathbb{R}^{n\times n}$. The system of partial differential equations given by equation (3.4) is called *hyperbolic at* (u, x, t) if the matrix $g(u, x, t)$ is diagonalisable with real eigenvalues. The system is called *hyperbolic* if g is hyperbolic for all $u \in \mathbb{R}^n, x \in X, t \in T$.

In this chapter we consider only hyperbolic systems.

Definition 3.2 (conservation). A system of partial differential equations is called conservative if it is of the following form:

$$u_{i,t}(x,t) + \left(f_i\left(u(x,t),x,t\right)\right)_{,x} = 0, \tag{3.5}$$

where $u : X \times T \to \mathbb{R}^n$ and $f : \mathbb{R}^n \times X \times T \to \mathbb{R}^n$ a so-called flux function.

Lemma 3.3. *A conservative system with flux function f independent of x is hyperbolic if the jacobian of f with respect to u is diagonalisable with real eigenvalues.*

Proof. Let $g(u,t)$ be the jacobian of $f(u,t)$ with respect to u:

$$g_{ij}(u,t) = f_{i,u_j}(u,t). \tag{3.6}$$

Then system (3.5) is equal to system (3.4). Hence, the former is hyperbolic if latter is. □

3.2.1 Uniqueness

It is well known [35] that a solution to a hyperbolic system may contain discontinuities, even when the initial and boundary conditions are continuous. At these discontinuities the differential equation (3.4) is undefined. As a consequence, multiple solutions may exist.

For example, consider the inviscid Burgers equation on an infinite domain, given by

$$u_{,t} + uu_{,x} = 0, \quad \text{for almost all } x \in \mathbb{R}, t \in \mathbb{R}^+. \tag{3.7}$$

This is clearly a hyperbolic differential equation. We will try to find solutions to this differential equation for the initial value

$$u(x,0) = \begin{cases} u_L & \text{if } x < 0, \\ u_R & \text{if } x > 0, \end{cases} \tag{3.8}$$

where $u_L < u_R \in \mathbb{R}$. We state the following two solutions; a justification will be given in the following sections: a shock moving with velocity $\frac{1}{2}(u_L + u_R)$,

$$u_{\text{shock}}(x,t) = \begin{cases} u_L & \text{if } x < \frac{1}{2}(u_L + u_R)\,t, \\ u_R & \text{if } x > \frac{1}{2}(u_L + u_R)\,t. \end{cases} \tag{3.9}$$

and a rarefaction wave,

$$u_{\text{rarefaction}}(x,t) = \begin{cases} u_L & \text{if } \frac{x}{t} < u_L, \\ u_R & \text{if } \frac{x}{t} > u_R, \\ \frac{x}{t} & \text{if } u_L < \frac{x}{t} < u_R. \end{cases} \tag{3.10}$$

It is easy to verify that both u_{shock} and $u_{\text{rarefaction}}$ satisfy the initial condition (3.8) and the differential equation (3.7). Hence, we have found two solutions for a single problem.

3.2.2 Parabolic regularisation

Which of the two solutions is correct? Without additional constraints the answer is both. The Burgers equation was originally defined with a viscous term:

$$u_{,t} + uu_{,x} = \epsilon u_{,xx}. \tag{3.11}$$

Solving this differential equation given the same initial value (3.8) does yield a unique solution. Letting the viscosity ϵ go to zero gives a unique solution to the inviscid differential equation.

The models discussed in Chapter 2 are derived from balance equations containing viscous terms as well. These terms are, however, neglected as they are assumed to be small. We may use the viscous terms to decide which of all solutions to the inviscid differential equation is the physically relevant one.

In absence of physical viscosity, an artificial viscosity term may be added to the hyperbolic system:

$$u_{i,t}(x,t) + g_{ij}(u(x,t),x,t)u_{j,x}(x,t) = \epsilon \left(\nu_{ij} u_{j,x}(x,t)\right)_{,x}, \tag{3.12}$$

where $\nu \in \mathbb{R}^{n\times n}$ is a nonzero viscosity matrix and $\epsilon > 0$ a small parameter. This is also called a *parabolic regularisation*. As in the examples above, the relevant solution is the limit of solutions to the parabolic differential equations for ϵ going to zero.

3.2.3 Entropy conditions

It can be quite difficult to use the parabolic regularisation to decide which solution is relevant, especially in numerical computations. Consider the following PDE,

$$u_{i,t} + \left(f\left(u\right)\right)_{i,x} = 0, \tag{3.13}$$

and the PDE with added viscosity,

$$\tilde{u}_{i,t} + \left(f\left(\tilde{u}\right)\right)_{i,x} = \epsilon \left(\nu_{ij}\left(\tilde{u},x,t\right)\tilde{u}_{j,x}\right)_{,x}. \tag{3.14}$$

Assume we have a function $\eta : \mathbb{R}^n \to \mathbb{R}$, called the *entropy function*, and a function $\psi : \mathbb{R}^n \to \mathbb{R}$, called the *entropy flux*, such that $\psi_{,j}\left(u\right) = \eta_{,i}\left(u\right) f_{i,j}\left(u\right)$ for all $u \in \mathbb{R}$. Multiplying the viscous conservative system (3.14) with $\eta_{,i}\left(\tilde{u}\right)$ gives

$$\eta_{,i}\left(\tilde{u}\right)\left(\tilde{u}_{i,t} + \left(f\left(\tilde{u}\right)\right)_{i,x}\right) = \epsilon\eta_{,i}\left(\tilde{u}\right)\left(\nu_{ij}\left(\tilde{u},x,t\right)\tilde{u}_{j,x}\right)_{,x}, \tag{3.15}$$

which can be written as

$$\begin{aligned}&\left(\eta_i\left(\tilde{u}\right)\right)_{,t} + \left(\psi\left(\tilde{u}\right)\right)_{,x}\\ &\qquad = \epsilon\left(\eta_{,i}\left(\tilde{u}\right)\nu_{ij}\left(\tilde{u},x,t\right)\tilde{u}_{j,x}\right)_{,x} - \epsilon\eta_{,ik}\left(\tilde{u}\right)\tilde{u}_{k,x}\nu_{ij}\left(\tilde{u},x,t\right)\tilde{u}_{j,x}.\end{aligned} \tag{3.16}$$

Integration over a rectangle $(x_1,x_2)\times(t_1,t_2)\subset X\times T$ gives

$$\begin{aligned}\int_{x_1}^{x_2}\left[\eta\left(\tilde{u}\right)\right]_{t=t_1}^{t_2}\,\mathrm{d}x + \int_{t_1}^{t_2}\left[\psi\left(\tilde{u}\right)\right]_{x=x_1}^{x_2}\,\mathrm{d}t &= \epsilon\int_{t_1}^{t_2}\left[\eta_{,i}\left(\tilde{u}\right)\nu_{ij}\left(\tilde{u},x,t\right)\tilde{u}_{j,x}\right]_{x=x_1}^{x_2}\,\mathrm{d}t\\ &\quad - \epsilon\int_{x_1}^{x_2}\int_{t_1}^{t_2}\eta_{,ik}\left(\tilde{u}\right)\tilde{u}_{k,x}\nu_{ij}\left(\tilde{u},x,t\right)\tilde{u}_{j,x}\,\mathrm{d}t\,\mathrm{d}x.\end{aligned} \tag{3.17}$$

If we let the viscosity vanish, be means of letting ϵ go to zero, the first integral on the right hand side will vanish [35]. If we are able to assert that the second integral on the right hand side is always nonnegative (for positive ϵ, hence in the limit for $\epsilon \to 0$, if existing), then we obtain the following condition for entropy solutions u of the inviscid system of differential equations (3.13):

$$\int_{x_1}^{x_2} \left[\eta\left(u\right)\right]_{t=t_1}^{t_2} \, \mathrm{d}x + \int_{t_1}^{t_2} \left[\psi\left(u\right)\right]_{x=x_1}^{x_2} \, \mathrm{d}t \leq 0, \quad \forall (x_1, x2) \subset X, (t_1, t_2) \subset T. \tag{3.18}$$

We can achieve this by an extra constraint on η: the matrix $\eta_{,ik}\nu_{ij}$ should be (strictly) positive definite,

$$\eta_{,ik}\left(v\right)\nu_{ij}\left(v,x,t\right)w_j w_k > 0, \quad \forall v, w \in \mathbb{R}^n, \ \|w\|_1 \neq 0. \tag{3.19}$$

Note that this requires $\nu_{ij}\left(v\right)$ to be an invertible matrix for all $v \in \mathbb{R}^n$.

To summarise, we have the following definition.

Definition 3.4 (entropy solution, conservative case). Let $\nu_{ij} : \mathbb{R}^n \to \mathbb{R}^{n\times n}$ be such that $\nu_{ij}\left(v\right)$ is an invertible matrix for all $v \in \mathbb{R}^n$ and let $\eta, \psi : \mathbb{R}^n \to \mathbb{R}$ be functions such that $\psi_{,j}\left(v\right) = \eta_{,i}\left(v\right) f_{i,j}\left(v\right), \forall v \in \mathbb{R}^n$ and such that η satisfies condition (3.19). A weak solution $u : X \times T \to \mathbb{R}^n$ to the inviscid system (3.13) is called an *entropy solution* (with respect to η, ψ and ν) if it satisfies condition (3.18).

For the general case, i.e. not limited to conservative systems, the entropy condition is more difficult. We repeat an entropy condition given by LeFloch [34], which is compatible with the conservative condition. Consider the following hyperbolic system,

$$u_{i,t} + g_{ij}\left(u\right)u_{j,x} = 0, \tag{3.20}$$

where $u(x,t) : X \times T \to U$ and $g(u,x,t) : U \times X \times T \to \mathbb{R}^n$, and the parabolic regularisation using viscosity matrix $\nu(u,x,t) : U \times X \times T \to \mathbb{R}^{n\times n}$,

$$\tilde{u}_{i,t} + g_{ij}\left(\tilde{u}\right)\tilde{u}_{j,x} = \epsilon\left(\nu_{ij}\left(\tilde{u},x,t\right)\tilde{u}_{j,x}\right)_{,x}, \quad \epsilon > 0, \tag{3.21}$$

where $\tilde{u}(\epsilon,x,t) : \mathbb{R} \times X \times T \to U$ is the viscous solution.

Instead of defining an entropy function $\eta(u) : U \to \mathbb{R}$, we define a vector $\gamma(u) : U \to \mathbb{R}^n$, comparable to $\eta_{,i}$ but we will discuss this later. Multiplying the viscous system (3.21) with γ_i yields

$$\gamma_i\left(\tilde{u}\right)\left(\tilde{u}_{i,t} + g_{ij}\left(\tilde{u},x,t\right)\tilde{u}_{i,x}\right) = \epsilon\gamma_i\left(\tilde{u}\right)\left(\nu_{ij}\left(\tilde{u},x,t\right)\tilde{u}_{j,x}\right)_{,x}, \tag{3.22}$$

Rearranging the right hand side yields

$$\begin{aligned}\gamma_i\left(\tilde{u}\right)\tilde{u}_{i,t} + \gamma_i\left(\tilde{u}\right)g_{ij}\left(\tilde{u},x,t\right)\tilde{u}_{i,x} \\ = \epsilon\left(\gamma_i\left(\tilde{u}\right)\nu_{ij}\left(\tilde{u},x,t\right)\tilde{u}_{j,x}\right)_{,x} - \epsilon\gamma_{i,k}\left(\tilde{u}\right)\tilde{u}_{k,x}\nu_{ij}\left(\tilde{u},x,t\right)\tilde{u}_{j,x}.\end{aligned} \tag{3.23}$$

If we let ϵ go to zero, then the first term on the right hand side vanishes. If we assert that the second term on the right side is always nonnegative, then we obtain the following condition:

$$\gamma_i\left(\tilde{u}\right)\tilde{u}_{i,t} + \gamma_i\left(\tilde{u}\right)g_{ij}\left(\tilde{u},x,t\right)\tilde{u}_{i,x} \leq 0, \tag{3.24}$$

which should hold in the weak sense. This can be achieved by the following condition on γ:

$$\gamma_i\left(v\right)\nu_{ij}\left(v,x,t\right)w_j w_k > 0, \quad \forall v, w \in \mathbb{R}^n, \ \|w\|_1 \neq 0. \tag{3.25}$$

In case the general system is conservative, then we would like to recover the conservative entropy condition, hence there should exist functions $\eta, \psi : U \to \mathbb{R}$ such that $\eta_{,i}(v) = \gamma_i(v)$ and $\psi_{,j}(v) = \gamma_i g_{ij}(v)$ for all $v \in U$. The following lemma ...

Proposition 3.5. *Let $f : U \to \mathbb{R}$ and $g_{ij} = f_{i,j}$. If γ satisfies*

$$\gamma_{i,j}(v) = \gamma_{j,i}(v), \quad \forall v \in U \tag{3.26}$$

and

$$\gamma_{i,j}(v)\, g_{jk}(v) = \gamma_{k,j}(v)\, g_{ji}(v), \quad \forall v \in U \tag{3.27}$$

then there exist functions $\eta, \psi : U \to \mathbb{R}$ such that $\eta_{,i}(v) = \gamma_i(v)$ and $\psi_{,j}(v) = \eta_{,i}(v)\, f_{i,j}(v)$ for all $v \in U$.

For a proof we refer the reader to LeFloch [34].

To summarise, we have the following definition.

Definition 3.6 (entropy solution, general case). Let $\nu_{ij} : \mathbb{R}^n \to \mathbb{R}^{n\times n}$ be such that $\nu_{ij}(v)$ is an invertible matrix for all $v \in \mathbb{R}^n$ and let $\gamma : \mathbb{U} \to \mathbb{R}^n$ be a function satisfying conditions (3.25), (3.26) and (3.27). A weak solution $u : X \times T \to \mathbb{R}^n$ to the inviscid system (3.20) is called an *entropy solution* (with respect to γ and ν) if it satisfies condition (3.24).

We now claim that both entropy conditions are equivalent for conservative systems:

Corollary 3.7. *Both entropy conditions (3.18) and (3.24) are equal (in the weak sense) when $g : U \to \mathbb{R}^{n\times n}$ is the jacobian of a function $f : U \to \mathbb{R}^n$.*

Proof. This follows immediately from Proposition 3.5. □

3.2.4 Riemann Problem

Consider the following Riemann Problem for the non-conservative hyperbolic PDE (3.4) on $\Omega = \mathbb{R}$ with $s = 0$,

$$u^0(x) = \begin{cases} u^L & : x < 0, \\ u^R & : x > 0. \end{cases} \tag{3.28}$$

In the following two sections we give two different solutions to the Riemann problem. An entropy condition can be used to decide which of both is the valid solution.

3.2.5 Rarefaction Waves

A rarefaction wave is a smooth solution to the Riemann problem. Assume the solution u is constant for fixed $\frac{x}{y} =: \xi$,

$$u(x,t) = \tilde{u}\left(\frac{x}{t}\right) = \tilde{u}(\xi). \tag{3.29}$$

Substituting in (3.4) yields

$$g_{ij}(\tilde{u}(\xi))\, \tilde{u}_{j,\xi}(\xi) = \xi \tilde{u}_{i,\xi}(\xi), \tag{3.30}$$

which is an eigenvalue problem with ξ being an eigenvalue and $\tilde{u}_{i,\xi}$ an eigenvector.

Define ξ as

$$\xi = \lambda(\tilde{u}(\xi)), \tag{3.31}$$

and $\tilde{u}(\xi)$ as

$$\tilde{u}_i(\xi) = \alpha(\xi)\, r_i(\tilde{u}(\xi)), \tag{3.32}$$

where $\lambda(u)$ is an eigenvalue of $g(u)$ and $r_i(u)$ a corresponding eigenvector and α a parameter. Then (3.30) is satisfied.

Taking the derivative of the eigenvalue with respect to ξ and substituting (3.32) gives

$$1 = \lambda_{,j}\left(\tilde{u}\left(\xi\right)\right)\tilde{u}_{j,\xi}\left(\xi\right) = \lambda_{,j}\left(\tilde{u}\left(\xi\right)\right)\alpha\left(\xi\right)r_j\left(\tilde{u}\left(\xi\right)\right), \tag{3.33}$$

which can be solved for α if $\lambda_{,j}\left(\xi\right)r_j\left(\tilde{u}\left(\xi\right)\right) \neq 0$. Substituting α in (3.32) gives a differential equation for the solution of the Riemann problem:

$$\tilde{u}_{i,\xi}\left(\xi\right) = \frac{r_i\left(\tilde{u}\left(\xi\right)\right)}{\lambda_{,j}\left(\tilde{u}\left(\xi\right)\right)r_j\left(\tilde{u}\left(\xi\right)\right)}. \tag{3.34}$$

3.2.6 Shock Waves

Alouges and Merlet [1] gave the following definition for a shock curve for the non-conservative system, based on a vanishing viscosity (3.12) where the viscosity matrix ν commutes with the jacobian matrix g.

Definition 3.8 (Alouges-Merlet Shock Curve). Assume the k-th is genuinely nonlinear. Let λ and r be the eigenvalue and eigenvector, respectively, of the k-th field. The approximate k-shock curve starting from u^{L} A nonconstant solution to

$$\begin{cases} \left(g_{ij}(u^{\mathrm{R}}) - \sigma\delta_{ij}\right)u^{\mathrm{R}}_{j,\sigma} = u^{\mathrm{R}}_i - u^{\mathrm{L}}_i, \\ u^{\mathrm{R}}(\lambda(u^{\mathrm{L}})) = u^{\mathrm{L}}, \end{cases} \tag{3.35}$$

for σ in the neighbourhood of $\lambda(u^{\mathrm{L}})$ is called an *approximate k-shock curve* of (3.4).

Chalmers and Lorin [10] defined an approximate solution of the shock curve.

Lemma 3.9. *An approximate solution to (3.35) is given by*

$$u^R_i(\sigma) = u^L_i + \frac{2(\sigma - \lambda(u^L))}{\lambda_{,j}(u^L)r_j(u^L)}r_i(u^L) + \frac{4(\sigma - \lambda(u^L))^2}{(\lambda_{,j}(u^L)r_j(u^L))^2}r_{i,j}(u^L)r_j(u^L) + \mathcal{O}(|\sigma - \lambda(u^L)|^3). \tag{3.36}$$

Proof. See Chalmers and Lorin [10]. □

3.3 Weak formulation

We follow the approach of Rhebergen, Bokhove and Van der Vegt [44] to obtain a weak formulation for the non-conservative hyperbolic PDE. The weak formulation is based on the DLM-measure named after Dal Maso, LeFloch and Murat [13]. This measure gives a meaning to products of functions with discontinuities and their derivatives by introducing a path connecting the discontinuities and integrating over this path. We repeat the definition of the path and measure.

Definition 3.10 (Integration paths, [13]). A Lipschitz continuous path $\phi : [0,1] \times \mathbb{R}^n \times \mathbb{R}^n \to \mathbb{R}^n$ is called an integration path if it satisfies the following properties:

$$\phi_i(0;q,v) = q_i \quad \text{and} \quad \phi_i(1;q,v) = v_i \quad \forall i \in \mathcal{I}, \forall q, v \in \mathbb{R}^n, \tag{3.37}$$

$$\phi_i(\tau;q,q) = q_i \quad \forall i \in \mathcal{I}, \forall q \in \mathbb{R}^n, \tag{3.38}$$

$$|\phi_{i,\tau}(\tau;q,v)| \leq K\left|q_i - v_i\right| \quad \forall i \in \mathcal{I}, \forall q, v \in \mathbb{R}^n, \tau \text{ a.e. } \in [0,1]. \tag{3.39}$$

Theorem 3.11 (DLM measure, [13]). *Let $q : (a, b) \to \mathbb{R}^n$ be a function of bounded variation and $f : \mathbb{R}^n \to \mathbb{R}^n$ be a continuous function. Then there exists a unique real-valued bounded Borel measure μ on (a, b) characterised by the two following properties:*

1. *If q is continuous on a Borel set $B \subset (a, b)$, then*

$$\mu_i(B; f, q) = \int_B f_{ij}(q) q_{i,x} \, d\lambda(x), \quad \forall i \in \mathcal{I}, \tag{3.40}$$

   where λ is the Borel measure.

2. *If q is discontinuous at a point $x \in (a, b)$, then*

$$\mu_i(\{x\}; f, q) = \int_0^1 f_{ij}(\phi(\tau; q(x^-), q(x^+)) \phi_{j,\tau}(\tau; q(x^-), q(x^+)) \, d\lambda(\tau), \quad \forall i \in \mathcal{I}, \tag{3.41}$$

   where $q(x^-) := \lim_{y \nearrow x} q(y)$ and $q(x^+) = \lim_{y \searrow x} q(y)$.

Consider the following PDE

$$u_{i,t} + (f_i(u))_{,x} + s_i = 0. \tag{3.42}$$

We obtain a weak formulation by multiplying the PDE (3.42) with a test function v and integrating the result using two different measures, a Lebesgue measure for the time derivative and source term and a DLM measure for the terms involving spatial derivatives, yielding

$$\int_\Omega v(x) \left(q_{i,x}(x,t) + s_i(q(x,t)) \right) d\lambda(x) + \int_\Omega v(x) \, d\mu_i(x; f, q) = 0, \quad \forall i \in \mathcal{I}. \tag{3.43}$$

The DG-FEM formulation follows from defining a set $\mathcal{E}$ of open, connected, nonoverlapping elements such that $\cup\mathcal{E}$ is dense in Ω, a broken polynomial space Q and assuming $q, v \in Q$. Let $\mathcal{D}$ denote the set of element edges, including any boundaries. Substituting the continuous (3.40) and discontinuous (3.41) definitions of the DLM measure yields the semi-discrete DG-FEM formulation

$$\sum_{E \in \mathcal{E}} \int_E v(x) \left(q_{i,t}(x,t) + s_i(q(x,t)) + f_{ij}(q(x,t)) q_{j,x}(x,t) \right) d\lambda(x) + \sum_{x \in \mathcal{D}} v(x) \int_0^1 f_{ij}(\phi(\tau; q(x^-,t), q(x^+,t))) \phi_{j,\tau}(\tau; q(x^-,t), q(x^+,t))) \, d\lambda(\tau) = 0, \quad \forall i \in \mathcal{I}. \tag{3.44}$$

Since the DLM measure is nonzero on element edges, the trial function v needs to have a (single) value at these points. We define this value by comparing the scheme with conventional DG-FEM schemes for conservative hyperbolic PDE's. Let $[\![q]\!] := x \mapsto q(x^+) - q(x^-)$ denote the jump of q at x and $\{\!\{q\}\!\} := x \mapsto \frac{1}{2}(q(x^+) + q(x^-))$ the average. Assuming the non-conservative part of f to be zero, $f_{\mathrm{n}} = 0$, the DG-FEM formulation (3.44) becomes

$$\sum_{E \in \mathcal{E}} \int_E v(x) \left(q_{i,t}(x,t) + s_i(q(x,t)) + F_{\mathrm{c},i}(q(x,t))_{,x} \right) d\lambda(x) + \sum_{x \in \mathcal{D}} v(x) \left[\!\left[F_{\mathrm{c},i}(q(\cdot,t)) \right]\!\right](x) = 0, \quad \forall i \in \mathcal{I}. \tag{3.45}$$

By asserting $v = \{\!\{v\}\!\}$ and applying integration by parts to the flux term in the element integral we obtain an unstable, conservative DG-FEM scheme with central fluxes:

$$\sum_{E\in\mathcal{E}} \int_E v(x)\left(q_{i,t}(x,t) + s_i(q(x,t)) - v_{,x}(x)F_{\mathrm{c},i}(q(x,t))\right) d\lambda(x) \\ - \sum_{x\in\mathcal{D}} [\![v]\!](x)\, \{\!\{F_{\mathrm{c},i}(q(\cdot,t))\}\!\}(x) = 0, \quad \forall i \in \mathcal{I}. \quad (3.46)$$

3.4 Stability

Due to the central approximation of the flux at element edges, the semi-discrete ODE (3.44) is unstable. There are various methods to stabilise the ODE, mostly originating from Finite Volume Methods, varying in the amount of added dissipation. Usually the less computationally demanding methods add the largest amount of dissipation, which often severely reduces the accuracy of low-order Finite Volume Methods. A high-order DG-FEM discretisation suffers far less from numerical dissipation [11]. For this reason, we prefer a cheap stabilisation method.

3.4.1 Rusanov

The Rusanov stabilisation is an example of a cheap and dissipative method. In Castro et al. [9] Rusanov stabilisation is derived for a non-conservative FVM. The equivalent of this stabilisation for a DG-FEM scheme is given by the following term, to be added to the right hand side of the semi-discrete ODE (3.44):

$$\mathrm{stab}_i := -\frac{1}{2}\sum_{x\in\mathcal{D}} C(q(x^-,t), q(x^+,t))\,[\![v]\!](x)\,[\![q_i(\cdot,t)]\!](x), \quad \forall i \in \mathcal{I}. \quad (3.47)$$

The function C determines locally, i.e. at each interface, the amount of added viscosity and should be larger than the absolute eigenvalues of the flux function g at the interface.

3.5 Discontinuous solutions

Strong oscillations may occur in a large area (spreading across multiple elements) around a discontinuity, possibly leading to an unstable situation, for instance when a solution becomes nonphysical. Persson and Peraire [39] proposed a technique to suppress the oscillations by adding viscosity locally and only when necessary. We repeat a short description of the method.

We add a viscous term to the original PDE (3.42) as follows:

$$u_{i,t} + f_{ij}(u)u_{j,x} + s_i(u) = \left(\epsilon u_{i,x}\right)_{,x}, \quad \forall i \in \mathcal{I}, \quad (3.48)$$

where ϵ is a parameter controlled by a shock sensor. As noted in Cockburn and Shu [11] discretisation of this PDE with the DG-FEM as described above by regarding $\epsilon u_{i,x}$ as a flux function may lead to an inconsistent scheme. The *local DG* [12] method is introduced to circumvent this. The PDE (3.48) is written as a (larger) system of first order derivatives by introducing the intermediate variable w_i,

$$u_{i,t} + f_{ij}(u)u_{j,x} + s_i(u) = \left(\epsilon w_i\right)_{,x}, \quad \forall i \in \mathcal{I}, \quad (3.49)$$

where w_i is defined as

$$w_i - u_{i,x} = 0, \quad \forall i \in \mathcal{I}. \tag{3.50}$$

There are other choices possible for this splitting, e.g. the viscosity could be incorporated in w_i, however, we observed that system (3.49), (3.50) produces the most stable and sharp results.

We discretise the viscous system (3.49), (3.50) in a similar way as described above. The PDE's are multiplied by a test function $v \in Q$ and integrated over the domain using the DLM measure for all spatial derivatives, including the split viscous terms, and the Lebesgue measure for the remaining terms:

$$\int_\Omega v(x) \left(q_{i,t}(x,t) + s_i(q(x,t),x,t)\right) \, d\lambda(x) + \int_\Omega v(x) \, d\mu_i(x; f, q) = \int_\Omega v(x) \, d\mu_i(x; \delta, \epsilon w) + \text{stab}_i, \quad \forall i \in \mathcal{I}, \tag{3.51}$$

$$\int_\Omega v(x) w_i(x,t) \, d\lambda(x) - \int_\Omega v(x) \, d\mu_i(x; \delta, u) = 0, \quad \forall i \in \mathcal{I}. \tag{3.52}$$

Note that for conservative fluxes, in this case (ϵw_i) , x and $u_{i,x}$, the DLM measure on discontinuous points is equivalent to a central flux. No additional stabilisation is required since the derivatives combined represent a second order derivative.

The amount of viscosity ϵ is determined by a shock sensor. We use the shock sensor as described in Persson and Peraire [39] with a minor modification. The shock sensor is applied to the sum of the internal energy for each phase, projected on Q, denoted by z. The highest mode of z at element E is measured against $z - z_{E1}$, the quantity with zero average value:

$$S_E = \frac{\int_E \hat{z}_{EP}^2 \psi_{EP}^2(x) \, d\lambda(x)}{\int_E (z - z_{E1})^2(x) \, d\lambda(x)}. \tag{3.53}$$

We use the same algorithm for obtaining a viscosity as described in Persson and Peraire [39] using the above shock sensor S_E.

3.6 Temporal integration

The time-dependent ODE's obtained after discretising the spatial part of a PDE can be solved with various explicit and implicit ODE solvers. We discuss one important family of solvers: the Runge-Kutta methods.

Consider the following nonlinear PDE:

$$u_{,t} = \mathcal{L}(u). \tag{3.54}$$

The general Runge-Kutta method is characterised by the following system of equations [11]:

$$v_i = \alpha_{ij} v_j + \Delta t \beta_{ij} \mathcal{L}(v_j), \tag{3.55}$$

where α_{ij} and β_{ij}, $i, j \in \{0, 1, \ldots, n\}$ are coefficients. Given an initial value v_0 at time t, solving the system yields an approximate solution v_n at time $t + \Delta t$. This procedure can be repeated by solving system (3.55) again using v_n of the previous solution as initial value v_0. Note that Δt need not be constant.

The Runge-Kutta method is explicit, in the sense that each intermediate step v_i depends only on the previous steps $v_j, j < i$, if the coefficients α_{ij} satisfy

$$\alpha_{ij} = 0 \, \forall j \geq i. \tag{3.56}$$

In the following we limit the discussion to scalar, one-dimensional ODE's. Total variation of the local means is defined as

$$|u|_{TV} = \sum_j \left| \int_{E_{j+1}} u \, \mathrm{d}x - \int_{E_j} u \, \mathrm{d}x \right|. \tag{3.57}$$

A Runge-Kutta method is stable when the total variation of the local means does not increase for each intermediate time step:

$$|v_{i+1}|_{TV} \leq |v_i| \, . \tag{3.58}$$

If the ODE does not satisfy this condition no matter how small the time step, we may apply a slope limiter $\Lambda\Pi$ to enforce this:

$$v_{ki} = \Lambda\Pi \left(\alpha_{ij} v_{kj} + \Delta t \beta_{ij} \mathcal{L} \left(v_{kj} \right) \right). \tag{3.59}$$

Cockburn and Shu [11] showed that the Runge-Kutta method is indeed stable when using a slope limiter and the following CFL-condition: at each time step k and each edge $j + \frac{1}{2}$ the following condition should hold,

$$c\Delta t \left(\frac{|f^* \left(a, \cdot \right)|_{\text{Lip}}}{\delta_{j+1}} \frac{|f^* \left(\cdot, b \right)|_{\text{Lip}}}{\delta_{j+1}} \right) \leq \frac{1}{2}, \tag{3.60}$$

where $c \in \mathbb{R}$ a constant such that

$$|\beta_{ij}| \leq c\alpha_{ij} \quad \forall i, j. \tag{3.61}$$

For a general system of ODE's there is no equivalent stability result.

Chapter 4

Test problems

In this chapter we discuss several test problems. We have simulated the first two test problems (Sections 4.3 and 4.4) using an equal pressure model (Section 4.1) discretised with the non-conservative DG-FEM scheme and a fourth-order Runge-Kutta method (Section 4.2). The remaining test problems (Sections 4.5–4.8) have not been simulated due to stability problems. We will address this problem in a future report.

4.1 Model

We use the equal pressure model, as described in Section 2.4, without friction. The conservation of mass is given by

$$\left(A_\beta \rho\right)_{,t} + \left(A_\beta \left(u_x \rho\right)\right)_{,x} = 0, \tag{4.1}$$

and the conservation of momentum by

$$\left(A_\beta \left(\rho u_x\right)\right)_{,t} + \left(A_\beta \left(u_x \rho u_x + \overline{p}\right)\right)_{,x} - \hat{p}_{(LG)} \left(A_\beta 1\right)_{,x} - A_\beta \left(\rho\right) g \sin\left(\theta\right) = 0, \tag{4.2}$$

with the pressure at the interface $\hat{p}_{(LG)}$ given by Equation (2.76). To close the system, we assume the gas phase to be an ideal gas with sound velocity c_G,

$$\rho_G = c_G^{-2} p, \tag{4.3}$$

and for the liquid phase we use a linearisation of the density around a reference pressure p_{L0}, at which the density is ρ_{L0},

$$\rho_L = \rho_{L0} + c_L^{-2} \left(p - p_{L0}\right). \tag{4.4}$$

The coefficient c_L is the speed of sound at the reference pressure p_{L0}. Furthermore, the volume equation holds:

$$A_L \left(1\right) + A_G \left(1\right) = 1. \tag{4.5}$$

The model can be written in the following form,

$$q_{i,t} + F_c(q)_{i,x} + f_{n;ij}(q) q_{j,x} + s_i(q) = 0, \tag{4.6}$$

where $i \in \{1, 2, 3, 4\}$. The vector $q \in \mathbb{R}^4$ holds the conserved quantities:

$$q_i = \begin{bmatrix} A_L \left(\rho\right) \\ A_G \left(\rho\right) \\ A_L \left(\rho u\right) \\ A_G \left(\rho u\right) \end{bmatrix}. \tag{4.7}$$

To define the functions F_c, f_n and s, we need to assume averages of products and products of averages to be equal. This allows us to write e.g. the average velocity in phase L, $\overline{u}_L$, as

$$\overline{u}_L = \frac{q_3}{q_1}. \tag{4.8}$$

The functions $F_c : \mathbb{R}^4 \to \mathbb{R}^4$ and $f_n : \mathbb{R}^4 \to \mathbb{R}^{4\times 4}$ are, respectively, the conservative and non-conservative parts of the flux:

$$F_c(q) = \begin{bmatrix} q_3 \\ q_4 \\ \frac{q_3^2}{q_1} + \alpha_L(q)\overline{p}(q) \\ \frac{q_4^2}{q_2} + \alpha_G(q)\overline{p}(q) \end{bmatrix}, \tag{4.9}$$

and

$$f_n(q) = \begin{bmatrix} 0 & 0 & 0 & 0 \\ 0 & 0 & 0 & 0 \\ -\hat{p}_{(LG)}(q)\frac{\partial \alpha_L}{\partial q_1}(q) & -\hat{p}_{(LG)}(q)\frac{\partial \alpha_L}{\partial q_2}(q) & 0 & 0 \\ -\hat{p}_{(LG)}(q)\frac{\partial \alpha_G}{\partial q_1}(q) & -\hat{p}_{(LG)}(q)\frac{\partial \alpha_G}{\partial q_2}(q) & 0 & 0 \end{bmatrix}. \tag{4.10}$$

The volume fractions $\alpha_L := A_L(1)$, $\alpha_G := A_G(1)$ and the average pressure $\overline{p}$ and interface pressure $\hat{p}_{(LG)}$ are functions of q, for which we derive expressions below. Function $s : \mathbb{R}^4 \to \mathbb{R}^4$ represents the source terms:

$$s(q) = \begin{bmatrix} 0 \\ 0 \\ q_1 g \sin(\theta) \\ q_2 g \sin(\theta) \end{bmatrix}. \tag{4.11}$$

4.1.1 Pressure and volume fractions

In order to find expressions for the average pressure $\overline{p}$ and volume fractions α_L, α_G in terms of the quantities q_1 and q_2 we need the volume equation (4.5), the equations of state (4.3) and the (4.4) and the definition of q_1 and q_2:

$$q_1 = \alpha_L \overline{\rho}_L, \tag{4.12}$$

and

$$q_2 = \alpha_G \overline{\rho}_G. \tag{4.13}$$

We combine the five equations into the following quadratic equation for the pressure p:

$$\overline{p}^2 - \overline{p}\left(q_1 c_L^2 + q_2 c_G^2 + p_{L0} - \rho_{L0} c_L^2\right) + q_2 c_G^2 \left(p_{L0} - \rho_{L0} c_L^2\right) = 0. \tag{4.14}$$

After solving for $\overline{p}$ we can find the values for the volume fractions as follows:

$$\alpha_G = \frac{q_2 c_G^2}{\overline{p}}, \tag{4.15}$$

and

$$\alpha_L = 1 - \alpha_G. \tag{4.16}$$

From Equation (4.15) we can find the derivatives of the volume fractions to q_j:

$$\frac{\partial \alpha_G}{\partial q_1} = -\frac{q_2 c_G^2}{\overline{p}^2}\frac{\partial p}{\partial q_1} = -\frac{\partial \alpha_L}{\partial q_1}, \tag{4.17}$$

Table 4.1: Initial data for the shock tube test problem

	$x < 0\,\mathrm{m}$	$x > 0\,\mathrm{m}$
α_{water}	0.71	0.70
p	$265000\,\mathrm{Pa}$	$265000\,\mathrm{Pa}$
u_{water}	$1\,\mathrm{m\,s^{-1}}$	$1\,\mathrm{m\,s^{-1}}$
u_{air}	$65\,\mathrm{m\,s^{-1}}$	$50\,\mathrm{m\,s^{-1}}$

and

$$\frac{\partial \alpha_G}{\partial q_2} = \frac{c_g^2}{\overline{p}} - \frac{q_2 c_G^2}{\overline{p}^2}\frac{\partial p}{\partial q_2} - \frac{\partial \alpha_L}{\partial q_2}. \tag{4.18}$$

The derivatives of p to q_j can be obtained from (4.14).

Given the averaged quantities derived above we can compute the interface pressure as defined in Equation (2.76).

4.2 Discretisation

To discretise the model described above, we use the Weak formulation as described in Section 3.3, with a linear path connecting discontinuities:

$$\phi_i\left(\tau; q^-, q^+\right) = (1-\tau)\, q_i^- + \tau q_i^+, \tag{4.19}$$

where $q^-, q^+ \in \mathbb{R}^4$ are the states left and right of a discontinuity.

We apply the viscous regularisation as described in Section 3.5 to reduce oscillations in the neighbourhood of discontinuities.

The semi-discrete weak formulation is integrated in time using a five-stage, fourth-order, low-storage Runge-Kutta method [8].

4.3 Shock tube

The *large relative velocity shock tube* test problem [14] [53] is a Riemann problem with the following initial data: the liquid volume fraction jumps from 0.71 to 0.7 and the gas velocity from 65 to $50\,\mathrm{m\,s^{-1}}$, the pressure is constant at $2.65 \cdot 10^5\,\mathrm{Pa}$ and the liquid velocity is $1\,\mathrm{m\,s^{-1}}$. There is no gravity force. See also Table 4.1. This Riemann problem generates four shocks, two of them moving at relatively high velocities, the other two with low velocities.

Figure 4.1 shows the solution of the system at $t = 0.1\,\mathrm{s}$, discretised with the DG-FEM method as described in this paper with 6 and 24 elements, both having 8 basis functions per element. For comparison results obtained using the first order Roe FVM as described in Evje and Flåtten [14] is shown using 192 elements, the same amount of DOF's as for DG with 24 elements.

All three solutions attain the same shock speeds and intermediate levels in the eyeball-norm. Both DG-schemes show no signs of the Gibbs phenomenon on the global scale. Zooming in on the edges does reveal a slight oscillation. The size of the oscillations is related to the amount of viscosity added to the system and can be further reduced at the cost of less sharp shocks.

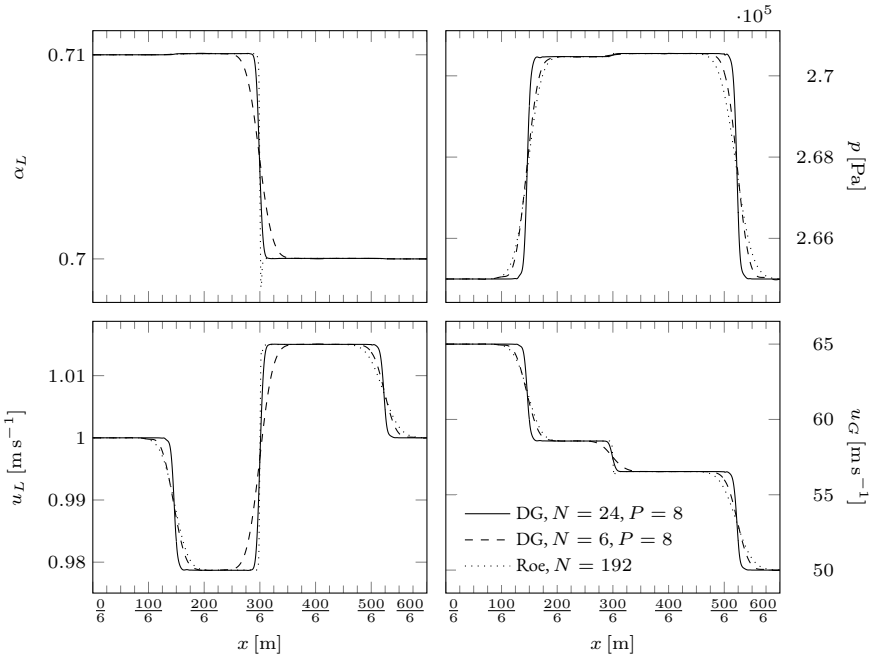

Figure 4.1: Results for the shock tube test problem at $t = 0.6$ s with 24 and 6 elements, all using 8 Legendre basis functions. Top-left: volume fraction water, top-right: pressure, bottom-left: velocity water, bottom-right: velocity air

4.4 Water faucet

The *water faucet test problem* [40] consists of a vertical pipe, 12m long, filled with a mixture of water (0.8 volume fraction) and air. Water flows initially with $10\ \mathrm{m\ s^{-1}}$ downwards, the air is at rest. At the top of the pipe the conditions are the same as the initial conditions. The bottom the pipe is at a constant pressure of 10^5 Pa. Under influence of gravity ($10\ \mathrm{m\ s^{-2}}$) the liquid will accelerate and the liquid fraction will decrease by conservation of mass. See also Table 4.2 and Figure 4.2.

Trapp and Riemke [52] derived the analytical solution to this problem with incompressible liquid and gas phase. The water velocity is given by

$$u_{\text{water}}(x,t) = \begin{cases} \sqrt{u_{\text{water}}^2(x,0) + 2gx} & : x < u_{\text{water}}(x,0)\, t + \frac{1}{2} g t^2, \\ u_{\text{water}}(x,0) + gt & : \text{otherwise.} \end{cases} \tag{4.20}$$

The water volume fraction is given by

$$\alpha_{\text{water}}(x,t) = \begin{cases} \alpha_{\text{water}}(x,0)\, \frac{u_{\text{water}}(x,0)}{u_{\text{water}}(x,t)} & : x < u_{\text{water}}(x,0)\, t + \frac{1}{2} g t^2, \\ \alpha_{\text{water}}(x,0) & : \text{otherwise.} \end{cases} \tag{4.21}$$

Since the pressure variation of the original model with compressible phases is small, this solution is considered to be a very good approximation to the system with compressible phases.

This test problem is discussed by Evje and Flåtten [14], Wangensteen [53], Toumi and Kumbaro [50] and Toumi, Kumbaro and Paillere [51].

Table 4.2: Initial and boundary conditions for the water faucet test problem

	$x = 0\,\mathrm{m}$	$0\,\mathrm{m} < x < 12\,\mathrm{m}$	$x = 12\,\mathrm{m}$
α_{water}	0.8	0.8	
p		$10^5\,\mathrm{Pa}$	$10^5\,\mathrm{Pa}$
u_{water}	$10\,\mathrm{m\,s^{-1}}$	$10\,\mathrm{m\,s^{-1}}$	
u_{air}	$0\,\mathrm{m\,s^{-1}}$	$0\,\mathrm{m\,s^{-1}}$	

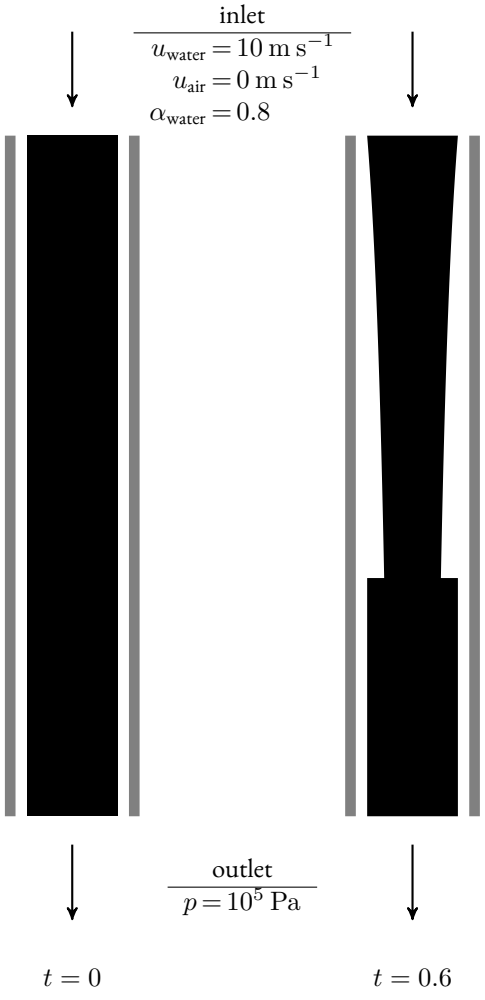

Figure 4.2: Illustration of the water faucet test problem at time $t = 0$ and $t = 0.6$. The black area denotes the water phase.

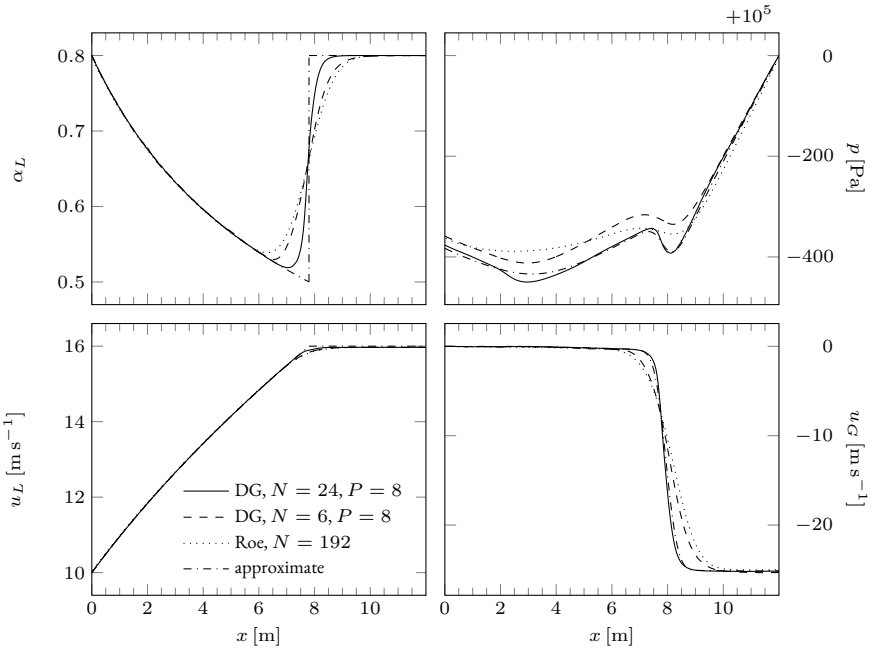

Figure 4.3: Results for the water faucet test problem at $t = 0.6$ s with 24 and 6 elements, all using 8 Legendre basis functions. Top-left: volume fraction water, top-right: pressure, bottom-left: velocity water, bottom-right: velocity air

Figure 4.3 shows the solution of the system at $t = 0.6$ s, discretised with the DG-FEM method as described in this paper with 6 and 24 elements, both having 8 basis functions per element. For comparison results obtained using the first order Roe FVM as described in Evje and Flåtten [14] is shown using 192 elements, the same amount of DOF's as for DG with 24 elements. Also the approximate solution is shown, which is based on the exact solution of the incompressible problem for the volume fraction and liquid velocity and a numerical solution of the Roe scheme with 1200 DOF's for the pressure and gas velocity.

The results are similar to the shock tube test problem. The Gibbs phenomenon is completely suppressed for both DG solutions, even on a small scale there are no wiggles present. The DG solutions converge to the approximate solution.

4.5 Separation

The separation test problem is designed to test the stability of the numerical schemes for the transition to and from single-phase flow. A vertical pipe of 7.5 m is closed on both sides and initially filled with a homogeneous mixture of water and air at rest. See also Table 4.3 for the initial and boundary conditions. Under influence of gravity, 'switched on' at $t = 0$ the, air will flow up and water down. Eventually both fluids are fully separated, i.e. the volume fractions are either zero or one almost everywhere.

This test problem is discussed by Evje and Flåtten [14] and Wangensteen [53].

Table 4.3: Initial and boundary conditions for the separation test problem

	$x = 0\,\mathrm{m}$	$0\,\mathrm{m} < x < 7.5\,\mathrm{m}$	$x = 12\,\mathrm{m}$
α_{water}		0.5	
p		$10^5\,\mathrm{Pa}$	
u_{water}	$0\,\mathrm{m\,s^{-1}}$	$0\,\mathrm{m\,s^{-1}}$	$0\,\mathrm{m\,s^{-1}}$
u_{air}	$0\,\mathrm{m\,s^{-1}}$	$0\,\mathrm{m\,s^{-1}}$	$0\,\mathrm{m\,s^{-1}}$

Table 4.4: Initial data and pipe angle ϕ for the oscillating manometer test problem

$x\,[\mathrm{m}]$	$x < -5$	$-5 < x < 5$	$5 < x$
$\phi\,[]$	$-\frac{1}{2}\pi$	$\frac{x}{10}\pi$	$\frac{1}{2}\pi$
$\alpha_{\text{water}}\,[]$	0	1	0
$u_{\text{water}}\,[\mathrm{m\,s^{-1}}]$	2.1	2.1	2.1
$u_{\text{air}}\,[\mathrm{m\,s^{-1}}]$	2.1	2.1	2.1

4.6 Oscillating manometer

The *oscillating manometer test problem*, introduced by Ransom [41] and discussed by discussed by Evje and Flåtten [14] and Wangensteen [53], is the multiphase pipe flow equivalent of a pendulum. A U-shaped tube is partially filled with water, under influence of gravity located at the bottom of the tube, and both water and air are given an initial uniform velocity. See Figure 4.4 for an illustration. Like a pendulum, the interaction between kinetic and gravity forces yields an oscillating flow.

The gravity force is included in the momentum source term:

$$g_x^{(\rho u)} := f_{\text{gravity}} \cos\phi, \tag{4.22}$$

where ϕ is the pipe inclination, see Table 4.4. Note that x denotes the position of the pipe, not an axis of a cartesian coordinate system. Note that this violates assumptions used for the derivation of the one-dimensional model. Evje and Flåtten [14] placed a virtual connection between both ends of the tube as to eliminate the need for boundary conditions.

4.7 Horizontal or near-horizontal pipe

A straight pipe with small or zero inclination θ is initially filled uniformly with liquid and gas flowing at velocity u_{sL0} and u_{sG0}, respectively. At the inlet the superficial velocity is kept constant: $u_{sL} = u_{sL0}$ and $u_{sG} = u_{sG0}$. At the outlet the pressure is equal to atmospheric pressure p_{atmos}. Depending on the inclination θ and the inlet velocities u_{sL0} and u_{sG0} slugs start to appear. We are interested in the transition surface in $(\theta, u_{sL0}, u_{sG0})$ from stratified to slug flow, the slug frequency and slug length distribution.

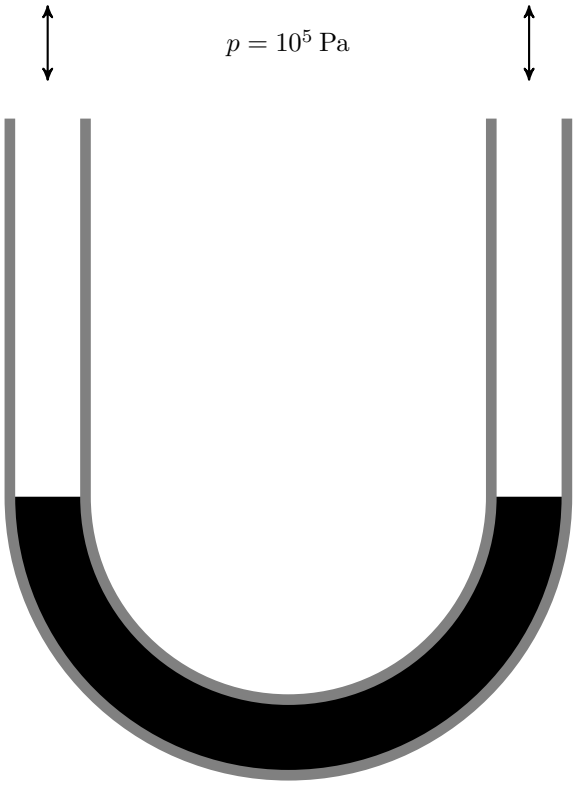

Figure 4.4: Illustration of the oscillating manometer test problem. The black area denotes the water phase.

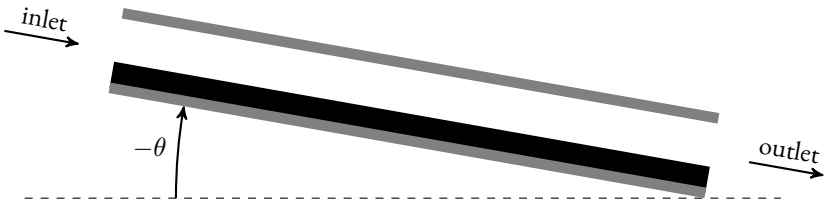

Figure 4.5: Illustration of the setup of the near-horizontal pipe test problem.The black area denotes the liquid phase.

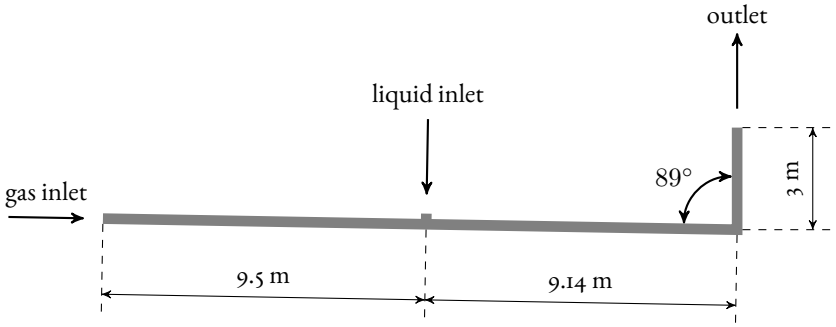

Figure 4.6: Illustration of the severe slugging cycle test problem

This test problem is discussed by Issa and Kempf [26] and Renault [43]. Experimental results are obtained by Woods, Hurlburt and Hanratty [55]. See also the references mentioned by Issa and Kempf [26] for more experimental results.

4.8 Severe slugging cycle

Flow lines including risers may produce severe slugging behaviour. Slugs form at the base of the riser, partially due to liquid flowing down, and, when accumulated enough mass, are blown out through the riser. This procedure repeats itself. The length and frequency of slugs and the appearance of slugs at all depend on the flow conditions. Roughly speaking, low superficial phase velocities will cause slugging, while high velocities will cause stable flow. For a comprehensive description of the meganism of slug flow in risers, see Seim et al. [46]

The following setup is used to examine severe slugging. The flow line consists of a 1deg downwards inclined section of $9.14\ \mathrm{m}$, followed by a riser of $3\ \mathrm{m}$. The pipe has diameter of $25.4\ \mathrm{mm}$. At the inlet there is a gas buffer of $0.0048\ \mathrm{m}^3$, which is equivalent to a flowline (with gas only) of $9.5\ \mathrm{m}$. At the inlet the mass flow of the two phases is varied to investigate the flow regime. At the outlet the pressure is equal to ambient pressure. See Figure 4.6 for an illustration.

This test problem is discussed by Jansen, Shoham and Taitel [27], Baliñoa, Burr and Nemoto [2], Taitel et al. [49], Sarica and Shoham [45] and Seim et al. [46].

Chapter 5

Conclusions

In this report we have given an overview of one-dimensional multiphase flow models and discretisation techniques for the simulation of long pipelines. The commonly used models and numerical schemes generation of models and numerical schemes are characterised by a coarse mesh and explicit modelling of flow regime transitions. More recently, the attention moved towards flow regime capturing schemes, where the multiphase flow model itself, with suitable choices for friction terms, is used to initiate the correct flow behaviour, provided that the discretisation is accurate enough. The slug capturing models require much more computational effort than the flow-regime based models.

The one-dimensional multiphase models are derived from three-dimensional conservation laws for mass, momentum and energy by averaging over the cross sectional area of the pipe per phase. This yields for each phase a set of conservation laws, connected by interface terms. The model is supplemented with relations for the friction at the interface and mass transfer, amongst others. Several simplifications have been suggested in literature: assuming a liquid phase to be incompressible and a slip relation which describes the relative motion of the phases, replacing a momentum balance for a single phase.

Many one-dimensional multiphase flow models are non-conservative, (conditionally) hyperbolic equations. It is not possible to derive a FVM or DG-FEM weak formulation in the traditional way when non-conservative products are present in the flux terms. A solution is provided in the form of a special measure, which gives a meaning to non-conservative products by introducing a path connecting the discontinuous points and integrating the non-conservative products along this path. The method is a generalisation of the traditional DG-FEM and FVM schemes. The correct choice for a path is not well defined.

Several stabilisation methods for FVM and DG-FEM schemes of conservative hyperbolic PDEs have been adapted to non-conservative PDEs. High-order methods require additional stabilisation to reduce oscillations within elements. An artificial viscosity term can be added to the system of PDEs, which locally adds diffusion when oscillations start to appear.

Such a DG-FEM scheme with artificial viscosity is applied to a two-fluid model and has been subjected to two test problems. The results compare well with an established scheme. No visible oscillations are present due to the artificial viscosity. The scheme fails on problems involving transitions from and to single phase flow

The scheme that we applied to several test problems has three major problems, which the author will address in the next period of his PhD project. Firstly, the scheme is unstable when there is a transition from and to single phase flow. Evje and Flåtten [14] have developed a FVM scheme which is unconditionally stable, by introducing a rather dissipative flux. We believe that combining the DG-FEM scheme in multiphase regions with a stable, first order

FVM scheme in transition regions is, at the moment, the most viable solution to stabilise our numerical scheme. The DG-FEM framework allows us to choose a (polynomial) basis per element. Choosing a basis consisting of a single, constant function is mathematically equivalent to a first order FVM scheme.

The second problem is the representation of shocks using high order polynomials, as used in DG-FEM schemes. Currently, we apply diffusion to eliminate the Gibbs phenomenon, at the cost of smearing of shocks. For other systems, better results have been reported by applying hp-refinement in combination with an error estimator controlling the refinement. For now, we propose to use a shock sensor to control the refinement in the following way: in the neighbourhood of shocks elements are subdivided and the order of the polynomial basis is reduced.

The third problem is the rather strict CFL condition of two-fluid systems discretised with DG-FEM and integrated in time using an explicit Runge-Kutta method. The oil and gas industry is less interested in accurately resolving the fast, sonic waves, which are the main cause of the strict CFL condition, but *is* interested in doing long simulations. We intend to circumvent the CFL condition by using a fully implicit time integration. While we could use an implicit Runge-Kutta method to integrate the semidiscrete DG-FEM scheme, we believe that using DGFEM for the time dimension as well has an advantage: the freedom/ability to use hp-refinement for space *and* time.

The resulting discrete system is nonlinear, both when using an implicit Runge-Kutta method or DG-FEM for the time dimension. We can solve this system using pseudo-time stepping, which involves adding a pseudo-time dimension and applying an explicit time integrator until the solution has converged in pseudo-time, or using Newton's method. Both methods have their advantages. We will investigate which method works best.

To summarise, in the next period the author will investigate the use of hp-refinement, both for resolving shocks and for stabilising the transition from and to single phase flow. To circumvent the strict CFL condition the author will apply space time DG-FEM and investigate methods to solve the resulting discrete, nonlinear system.

Bibliography

[1] F. Alouges and B. Merlet. 'Approximate Shock Curves for Non-Conservative Hyperbolic Systems in One Space Dimension'. *Journal of Hyperbolic Differential Equations* 1.4 (2004), pp. 769–788.

[2] J.L. Baliñoa, K.P. Burr and R.H. Nemoto. 'Modeling and simulation of severe slugging in air–water pipeline–riser systems'. *International Journal of Multiphase Flow* 36.8 (2010), pp. 643–660.

[3] F. Barre and M. Bernard. 'The CATHARE code strategy and assessment'. *Nuclear Engineering and Design* 124.3 (1990), pp. 257–284.

[4] K.H. Bendiksen et al. *The Dynamic Two-Fluid Model OLGA: Theory and Application*. Tech. rep. SPE/19451. Institutt for energiteknikk, 1991.

[5] D. Bestion. 'The Physical Closure Laws in the CATHARE Code'. *Nuclear Engineering and Design* 124.3 (1990), pp. 229–245.

[6] D. Biberg. 'A Mathematical Model for Two-Phase Stratified Turbulent Duct Flow'. *Multiphase Science and Technology* 19.1 (2007), pp. 1–48.

[7] M. Bonizzi, P. Andreussi and S. Banerjee. 'Flow regime independent, high resolution multi-field modelling of near-horizontal gas-liquid flows in pipelines'. *International Journal of Multiphase Flow* 35.1 (2009), pp. 34–46.

[8] M.H. Carpenter and C. Kennedy. *Fourth-Order 2N-Storage Runge-Kutta Schemes*. Tech. rep. TM 109112. NASA Langley Research Center, 1994.

[9] M.J. Castro et al. 'On Some Fast Well-Balanced First Order Solvers For Nonconservative Systems'. *Mathematics of Computation* 79.271 (2010), pp. 1427–1472.

[10] N. Chalmers and E. Lorin. 'Approximation of Nonconservative Hyperbolic Systems Based on Different Nonconservative Product Definitions'. *Canadian Applied Mathematics Quarterly* 17.3 (2009).

[11] B. Cockburn and C.W. Shu. 'Runge-Kutta Discontinuous Galerkin Methods for Convection-Dominated Problems'. *Journal of Scientific Computing* 16.3 (2001), pp. 173–261.

[12] B. Cockburn and C.W. Shu. 'The Local Discontinuous Galerkin Method for Time-Dependent Convection-Diffusion Systems'. *SIAM Journal on Numerical Analysis* 35.6 (1998), pp. 2440–2463.

[13] G. Dal Maso, P.G. LeFloch and F. Murat. 'Definition and Weak Stability of Nonconservative Products'. *Journal de Mathématiques Pures et Appliquées* 74.6 (1995), pp. 483–548.

[14] S. Evje and T. Flåtten. 'Hybrid Flux-Splitting Schemes for a Common Two-Fluid Model'. *Journal of Computational Physics* 192.1 (2003), pp. 175–210.

[15] S. Evje and T. Flåtten. 'Weakly Implicit Numerical Schemes for a Two-Fluid Model'. *SIAM Journal on Scientific Computing* 26.5 (2005), pp. 1449–1484.

[16] T. Flåtten. 'Hybrid Flux Splitting Schemes for Numerical Resolution of Two-Phase Flows'. PhD thesis. Norwegian University of Science and Technology (NTNU), 2003.

[17] R.A.W.M. Henkes, A.J.N. Vreenegoor Vreenegoor and G. Haandrikman. *Threephase Model for the Stratified Flow of Water, Oil and Gas in Pipelines*. Tech. rep. OP.98.20590. Shell International Oil Products B.V., 1998.

[18] J.S. Hesthaven and T. Warburton. *Nodal Discontinuous Galerkin Methods*. Texts in Applied Mathematics 54. Springer New York, 2008.

[19] H. Holmås. 'Numerical simulation of transient roll-waves in two-phase pipe flow'. *Chemical Engineering Science* 65.5 (2010), pp. 1811–1825.

[20] H. Holmås. 'Numerical simulation of waves in two-phase pipe flow using 1D two-fluid models'. PhD thesis. University of Oslo, 2008.

[21] H. Holmås, D. Clamond and H.P. Langtangen. 'A pseudospectral Fourier method for a 1D incompressible two-fluid model'. *International Journal for Numerical Methods in Fluids* 58.6 (2008), pp. 639–658.

[22] H. Holmås et al. 'Analysis of a 1D incompressible two-fluid model including artificial diffusion'. *IMA Journal of Applied Mathematics* 73.4 (2008), pp. 651–667.

[23] R.H.A IJzermans. 'On the Specifics of COMPAS'. private communication. 2011.

[24] M. Ishii. *Thermo-fluid Dynamic Theory of Two-Phase Flow*. Collection de la Direction des études et researches d'Electricité de France 22. Eyrolles, Paris, France, 1975.

[25] M. Ishii and T. Hibiki. *Thermo-Fluid Dynamics of Two-Phase Flow*. Springer Verlag, 2010.

[26] R.I. Issa and M.H.W. Kempf. 'Simulation of slug flow in horizontal and nearly horizontal pipes with the two-fluid model'. *International Journal of Multiphase Flow* 29.1 (2003), pp. 69–95.

[27] F.E. Jansen, O. Shoham and Y. Taitel. 'The Elimination of Severeslugging—Experiments and Modeling'. *International Journal of Multiphase Flow* 22.6 (1996), pp. 1055–1072.

[28] Guangshan Jiang and Chi-Wang Shu. 'On a Cell Entropy Inequality for Discontinuous Galerkin Methods'. *Mathematics of Computation* 62.206 (1994), pp. 531–538.

[29] Th. von Kármán. 'Mechanische Ähnlichkeit und Turbulenz'. *Nachrichten von der Gesellschaft der Wissenschaften zu Göttingen, Mathematisch-Physikalische Klasse* (1930), pp. 58–76.

[30] O. Kristiansen. 'Experiments on the Transition from Stratified to Slug Flow in Multiphase Pipe Flow'. PhD thesis. Norwegian University of Science and Technology (NTNU), 2004.

[31] M. Larsen et al. *PeTra: Model and Numerics Guide*. Tech. rep. IFE/KR/F-2002/101. Institutt for energiteknikk, 2002.

[32] H. Laux et al. 'Simulation of multiphase flows composed of large scale interfaces and dispersed fields'. *Proceedings of the 6th International Conference on Multiphase Flow*. 2007.

[33] A. De Leebeeck and O.J. Nydal. 'Simulation of Large Amplitude Waves in a Slug Tracking Scheme Compared to Roll Wave Experiments at High Pressure'. *International Journal of Multiphase Flow* 36.1 (2010), pp. 40–50.

[34] P.G. LeFloch. 'Entropy Weak Solutions to Nonlinear Hyperbolic Systems under Nonconservative Form'. *Communications in Partial Differential Equations* 13.6 (1988), pp. 669–727.

[35] R.J. LeVeque. *Finite volume methods for hyperbolic problems*. Cambridge University Press, 2002.

[36] M.-S. Liou and C.J. Steffen. 'A New Flux Splitting Scheme'. *Journal of Computational Physics* 107.1 (1993), pp. 23–39.

[37] L.F. Moody. 'Friction Factors for Pipe Flow'. *Transactions of the ASME* 66.8 (1944), pp. 671–684.

[38] Stanley Osher. 'Riemann Solvers, the Entropy Condition, and Difference Approximations'. *SIAM Journal on Numerical Analysis* 21.2 (1984), pp. 217–235.

[39] P.O. Persson and J. Peraire. 'Sub-Cell Shock Capturing for Discontinuous Galerkin Methods'. *Proceedings of the 44th AIAA Aerospace Sciences Meeting and Exhibit*. American Institute of Aeronautics and Astronautics, 2006.

[40] V.H. Ransom. 'Numerical Benchmark Test no. 2.1: Faucet Flow'. *Multiphase Science and Technology* 3 (1987), pp. 465–467.

[41] V.H. Ransom. 'Numerical Benchmark Test no. 2.2: Oscillating Manometer'. *Multiphase Science and Technology* 3 (1987), pp. 468–470.

[42] V.H. Ransom and D.L. Hicks. 'Hyperbolic Two-Pressure Models for Two-Phase Flow'. *Journal of Computational Physics* 53.1 (1984), pp. 124–151.

[43] F. Renault. 'A Lagrangian Slug Capturing Scheme for Gas-Liquid Flows in Pipes'. PhD thesis. Norwegian University of Science and Technology (NTNU), 2007.

[44] S. Rhebergen, O. Bokhove and J.J.W. Van der Vegt. 'Discontinuous Galerkin Finite Element Methods for Hyperbolic Nonconservative Partial Differential Equations'. *Journal of Computational Physics* 227.3 (2008), pp. 1887–1922.

[45] C. Sarica and O. Shoham. 'A simplified transient model for pipeline-riser systems'. *Chemical Engineering Science* 46.9 (1991), pp. 2167–2179.

[46] J.E. Seim et al. 'Experiments and Modelling for the Control of Riser Instabilities with Gas Lift'. *Proc. 15th Int. Conf. on Multiphase Prod. Technology*. 2011, pp. 19–31.

[47] B.H. Stewart and B. Wendroff. 'Two-phase Flow: Models and Methods'. *Journal of Computational Physics* 56.3 (1984), pp. 363–409.

[48] Y. Taitel and A.E. Dukler. 'A Model for Predicting Flow Regime Transitions in Horizontal and Near Horizontal Gas-Liquid Flow'. *AIChE Journal* 22.1 (1976), pp. 47–55.

[49] Y. Taitel et al. 'Severe slugging in a riser system: experiments and modeling'. *International Journal of Multiphase Flow* 16.1 (1990), pp. 57–68.

[50] I. Toumi and A. Kumbaro. 'An Approximate Linearized Riemann Solver For a Two-Fluid Model'. *Journal of Computational Physics* 124.2 (1996), pp. 286–300.

[51] I. Toumi, A. Kumbaro and H. Paillere. 'Approximate Riemann Solvers and Flux Vector Splitting Schemes for Two-Phase Flow'. *30th Computational Fluid Dynamics* (1999).

[52] J.A. Trapp and R.A. Riemke. 'A nearly-implicit hydrodynamic numerical scheme for two-phase flows'. *Journal of Computational Physics* 66.1 (1986), pp. 62–82.

[53] T. Wangensteen. 'Mixture-Slip Flux Splitting for the Numerical Computation of 1D Two Phase Flow'. PhD thesis. Norwegian University of Science and Technology (NTNU), 2010.

[54] P. Wesseling. *Principles of Computational Fluid Dynamics*. Springer Verlag, 2010.

[55] B.D. Woods, E.T. Hurlburt and T.J. Hanratty. 'Mechanism of slug formation in downwardly inclined pipes'. *International Journal of Multiphase Flow* 26.6 (2000), pp. 977–998.

[56] N. Zuber and J. A. Findlay. 'Average Volumetric Concentration in Two-Phase Flow Systems'. *Journal of Heat Transfer* 87.4 (1965), pp. 453–468.

Appendix A

Derivation entropy equation

The total energy E is related to internal energy e and velocity u as follows:

$$E = e + \tfrac{1}{2} u_i u_i. \tag{A.1}$$

Applying this to the left hand side of the energy balance (2.18) gives

$$\begin{aligned}(\rho E)_{,t} + (u_i \rho E)_{,i} &= E\left(\rho_{,t} + (u_i \rho)_{,i}\right) + \rho E_{,t} + u_i \rho E_{,i} \\ &= E\left(\rho_{,t} + (u_i \rho)_{,i}\right) + \rho e_{,t} + u_i \rho e_{,i} + \tfrac{1}{2}\rho \left(u_j u_j\right)_{,t} + \tfrac{1}{2} u_i \rho \left(u_j u_j\right)_{,i}. \end{aligned} \tag{A.2}$$

The last two terms can be written as

$$\begin{aligned}\tfrac{1}{2}\rho \left(u_j u_j\right)_{,t} + \tfrac{1}{2} u_i \rho \left(u_j u_j\right)_{,i} &= \rho u_j u_{j,t} + u_i \rho u_j u_{j,t} \\ &= u_j \left((\rho u_j)_{,t} + (u_i \rho u_j)_{,i}\right) - u_j u_j \left(\rho_{,t} + (u_i \rho)_{,i}\right). \end{aligned} \tag{A.3}$$

Entropy per unit mass is defined as [54]

$$T \delta s = \delta e - p \delta \frac{1}{\rho}, \tag{A.4}$$

where δ indicates small changes. The terms of (A.2) involving the internal energy e can be written as

$$\begin{aligned}\rho e_{,t} + u_i \rho e_{,i} &= T \rho s_{,t} + T u_i \rho s_{,i} + \frac{p}{\rho} \rho_{,t} + \frac{p}{\rho} u_i \rho_{,i} \\ &= T\left((\rho s)_{,t} + (u_i \rho s)_{,i}\right) + \left(\frac{p}{\rho} - T s\right)\left(\rho_{,t} + (u_i \rho)_{,i}\right) - p u_{i,i}. \end{aligned} \tag{A.5}$$

Combining (A.3) and (A.5) in (A.2) yields

$$\begin{aligned}(\rho E)_{,t} + (u_i \rho E)_{,i} = &\left(E + \frac{p}{\rho} - T s - u_j u_j\right)\left(\rho_{,t} + (u_i \rho)_{,i}\right) \\ &+ T\left((\rho s)_{,t} + (u_i \rho s)_{,i}\right) - p u_{i,i} + u_j \left((\rho u_j)_{,t} + (u_i \rho u_j)_{,i}\right). \end{aligned} \tag{A.6}$$

Substituting the balance laws (2.2)–(2.4) and applying Equation (2.5) yields the entropy equation:

$$T(\rho s)_{,t} + T(u_i \rho s)_{,i} = \left(E - 2e + sT - \frac{p}{\rho}\right) g^{(\rho)} + u_{i,j} \tau_{ij} + (k T_{,i})_{,i} + \rho g^{(\rho E)}. \tag{A.7}$$

Appendix B

DG-FEM

We discuss the Discontinuous Galerkin Finite Element Method (DG-FEM) by means of the following nonlinear, conservative, hyperbolic system of m PDEs on a d-dimensional domain $\Omega \subset \mathbb{R}^d, d \in \{1, 2, 3, \dots\}$,

$$u_{i,t} + f_{ij}(u)_{,j} = 0 \tag{B.1}$$

where $i \in \{1, 2, \dots, m\}$ is an index of the PDEs, $j \in \{1, 2, \dots, d\}$ an index of the spatial dimensions, $u_i \in U$, with U the set of piecewise continuous functions from $(x \in \Omega, t)$ to $\mathbb{R}$, and $f_{ij} := U \to \mathbb{R}$. We do not discuss boundary conditions in this chapter.

Let $\mathcal{E} \in \mathbb{R}^d$ be a set of open, non-overlapping, connected subsets, such that the union approximates Ω:

$$\tilde{\Omega} := \bigcup_{E \in \mathcal{E}} \overline{E} \approx \Omega. \tag{B.2}$$

The set of elements $\mathcal{E}$ defines a mesh on $\tilde{\Omega}$. Let $\tilde{U}$ be space of functions from $(x \in \Omega, t)$ to $\mathbb{R}$ such that every $u \in U$ is continuous on every $E \in \mathcal{E}$. Typically a space spanned by several polynomials per $E \in \mathcal{E}$ is used.

We replace u in the PDEs (B.1) with $\tilde{u} \in \tilde{U}$, multiply the result with a test function $v \in \tilde{U}$ and integrate over an element $E \in \mathcal{E}$,

$$\int_E (\tilde{v}\tilde{u}_{i,t} + \tilde{v} f_{ij}(\tilde{u})_{,j}) \, d\lambda = 0. \tag{B.3}$$

Applying partial integration to the flux term yields

$$\int_E (\tilde{v}\tilde{u}_{i,t} - \tilde{v}_{,j} f_{ij}(\tilde{u})) \, d\lambda + \int_{\partial E} \tilde{v} f_{ij} \left(\tilde{u}|_{\partial E} \right) n_j \, d\lambda = 0. \tag{B.4}$$

where n_j is the unit outward normal to the boundary ∂E. Note that the functions in $\tilde{U}$ are discontinuous at the boundary of E. The term $\tilde{u}|_{\partial E}$ denotes the trace of u taken from within E. Formally, we define $\tilde{u}|_{\partial E}$ at $x \in \partial E$ as the limit of $\tilde{u}(y)$, y going to x along a path inside E:

$$\tilde{u}|_{\partial E} := \overline{E} \ni x \mapsto \lim_{E \ni y \to x} \tilde{u}(y). \tag{B.5}$$

At this point there is no connection with neighbouring elements and, as a consequence, no global conservation. To solve this we replace the flux f in the boundary integral with the *numerical flux* f^*, which takes the values $\tilde{u}$ of both sides of an edge and returns a single flux value:

$$\int_E (\tilde{v}\tilde{u}_{i,t} - \tilde{v}_{,j} f_{ij}(\tilde{u})) \, d\lambda + \int_{\partial E} \tilde{v} f^*_{ij}(\tilde{u}) n_j \, d\lambda = 0. \tag{B.6}$$

We finally arrive at a DG-FEM scheme: find $u \in \tilde{U}$ such that for all $v \in \tilde{U}$,

$$\sum_{E\in\mathcal{E}} \int_E \left(\tilde{v}\tilde{u}_{i,t} - \tilde{v}_{,j} f_{ij}(\tilde{u})\right)\, d\lambda + \sum_{E\in\mathcal{E}} \int_{\partial E} \tilde{v} f^*_{ij}(\tilde{u}) n_j \, d\lambda = 0. \tag{B.7}$$

To implement this scheme we must choose a basis $\{p_k\}_k$ for $\tilde{U}$, describe the solution $\tilde{u}$ in terms of this basis,

$$\tilde{u}(x,t) = \hat{u}_k(t) p_k(x), \tag{B.8}$$

and evaluate the DG-FEM scheme (B.7) using test functions p_l:

$$\sum_{E\in\mathcal{E}} \int_E \left(p_l \hat{u}_{ki} p_{k,t} - p_{l,j} f_{ij}(\tilde{u})\right)\, d\lambda + \sum_{E\in\mathcal{E}} \int_{\partial E} p_l f^*_{ij}(\tilde{u}) n_j \, d\lambda = 0. \tag{B.9}$$

Rewriting this equation gives a system of time-dependent ODEs,

$$\hat{u}_{ki,t} = \sum_{E\in\mathcal{E}} M^{-1}_{kl} \int_E p_{l,j} f_{ij}(\tilde{u})\, d\lambda - \sum_{E\in\mathcal{E}} \int_{\partial E} p_l f^*_{ij}(\tilde{u}) n_j \, d\lambda, \tag{B.10}$$

where

$$M_{lk} := \sum_{E\in\mathcal{E}} \int_E p_l p_k \, d\lambda. \tag{B.11}$$

is the mass matrix.

We list several properties of the DG-FEM scheme (B.7):

- The DG-FEM scheme (B.7) has the following non-linear stability TODO: add eqn ref) has a strong nonlinear stability result for scalar hyperbolic equations [28]

  $$\frac{1}{2}\left(\|\tilde{u}\|_{\tilde{\Omega}}\right)_{,t} \leq 0, \tag{B.12}$$

  [28] provided that the numerical flux f^* is an E-flux [38]:

  $$\left(f^*(u^+,u^-) - f(u)\right)\left(u^+ - u^-\right) \leq 0, \quad \forall u \in [u^-, u^+]. \tag{B.13}$$

  $$\left(f^*_j(u) - f_j(w)\right)[\![u]\!]_j \leq 0, \tag{B.14}$$

  Furthermore, Jiang and Shu [28] show that the weak solution converges to the unique entropy solution if the weak solution is bounded and the flux f is convex.

- The DG-FEM scheme has a local conservation property. To see this, we substitute $v = 1$ in equation (B.6),

  $$\left(\int_E \tilde{u}_i \, d\lambda\right)_{,t} + \int_{\partial E} n_j f^*_{ij}(\tilde{u})\, d\lambda = 0, \quad \forall E \in \mathcal{E}. \tag{B.15}$$

  We assumed here that the mesh $\mathcal{E}$ does not change in time.

  Due to the numerical flux f^* being single valued (on element edges), we also have the global conservation. Before we prove this, we introduce the jump operator. On an edge e with normal n we define the jump of a function $u \in U$ as

  $$[\![u]\!]_j := e \ni x \mapsto \lim_{\epsilon\to 0^+} n_j \left(f(u(x+\epsilon n)) - f(u(x-\epsilon n))\right). \tag{B.16}$$

Note that $-n$ is also a normal of e, however, the jump operator is the same for n and $-n$. The jump operator can be interpreted as a gradient for discontinuities.

In equation (B.7), we collapse all boundary integrals occuring twice into a single integral by introducing a jump in $\tilde{v}$,

$$\sum_{E\in\mathcal{E}}\int_E \left(\tilde{v}\tilde{u}_{i,t} - \tilde{v}_{,j}f_{ij}(\tilde{u})\right)\,d\lambda - \sum_{e\in\bigcup_{E\in\mathcal{E}}\partial E\setminus\partial\tilde{\Omega}}\int_e [\![\tilde{v}]\!]_k\, n_k f^*_{ij}(\tilde{u})n_j\,d\lambda + \sum_{e\in\bigcup_{E\in\mathcal{E}}\partial E\cap\partial\tilde{\Omega}}\int_e \tilde{v}f^*_{ij}(\tilde{u})n_j\,d\lambda = 0. \quad \text{(B.17)}$$

The second summation iterates over all shared element edges, the third summation over the edges at the boundary of $\tilde{\Omega}$. Note that the solution at $\partial\tilde{\Omega}$ is single valued. Finally, let $v = 1$ on $\tilde{\Omega}$,

$$\left(\sum_{E\in\mathcal{E}}\int_E u_i\,d\lambda\right)_{,t} + \sum_{e\in\bigcup_{E\in\mathcal{E}}\partial E\cap\partial\tilde{\Omega}}\int_e f^*_{ij}(\tilde{u})n_j\,d\lambda = 0. \quad \text{(B.18)}$$

The jumps of $\tilde{v}$ vanish which causes all internal boundary integrals to vanish and we obtain global conservation.

- Basis functions have support on a single element. This implies that the mass matrix is block diagonal. It is, in general, cheap to compute the inverse, as needed for explicit timestepping of the semi-discrete formulation (B.7). When using an orthonormal basis, e.g. tensor products of normalised Legendre polynomials on orthotopes (hyperrectangles), the mass matrix is the identity matrix. An important consequence is that it is very easy and effective to parallelise the DG-FEM scheme.

  Due to the continuity of basis functions in CG-FEM, basis functions have support on multiple elements, yielding a mass matrix which is not block diagonal.

- The DG-FEM scheme is quite liberal in the choice of a mesh. A mesh with hanging nodes, see Figure B.1 for an example, are supported without any modification or special choice of basis functions. This is an important difference with continuous Galerking FEM, where either a special, continuous basis needs to be constructed or the mesh needs to be adjusted to eliminate the hanging nodes. Note that the latter is not possible when using a mesh of orthotopes, see Figure B.2. Furthermore, the DG-FEM scheme allows combinations of elements with different shapes.

- A DG-FEM scheme with only constant basis functions is equivalent to a Finite Volume Scheme.

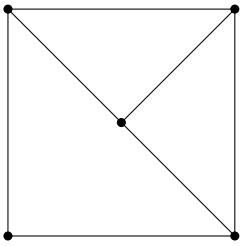

Figure B.1: An example of a mesh of triangles with a hanging node.

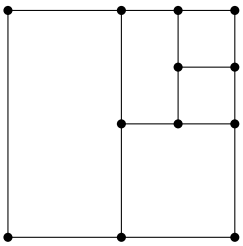

Figure B.2: An example of a mesh of rectangular elements with several hanging nodes.